J. Fluid Mech. (2010), *vol.* 645, *pp.* 27–57. © Cambridge University Press 2010
doi:10.1017/S0022112009992485

Analytical solutions for tsunami runup on a plane beach: single waves, N-waves and transient waves

PER A. MADSEN† AND HEMMING A. SCHÄFFER‡

Department of Mechanical Engineering, Technical University of Denmark, 2800 Kgs Lyngby, Denmark

(Received 30 July 2008; revised 21 September 2009; accepted 27 September 2009)

In the literature it has so far been common practice to consider solitary waves and N-waves (composed of solitary waves) as the appropriate model of tsunamis approaching the shoreline. Unfortunately, this approach is based on a tie between the nonlinearity and the horizontal length scale (or duration) of the wave, which is not realistic for geophysical tsunamis. To resolve this problem, we first derive analytical solutions to the nonlinear shallow-water (NSW) equations for the runup/rundown of single waves, where the duration and the wave height can be specified separately. The formulation is then extended to cover leading depression N-waves composed of a superposition of positive and negative single waves. As a result the temporal variations of the runup elevation, the associated velocity and breaking criteria are specified in terms of polylogarithmic functions. Finally, we consider incoming transient wavetrains generated by monopole and dipole disturbances in the deep ocean. The evolution of these wavetrains, while travelling a considerable distance over a constant depth, is influenced by weak dispersion and is governed by the linear Korteweg–De Vries (KdV) equation. This process is described by a convolution integral involving the Airy function. The runup on the plane sloping beach is then determined by another convolution integral involving the incoming time series at the foot of the slope. A good agreement with numerical model results is demonstrated.

1. Introduction

Analytical runup expressions for various wave forms such as periodic waves, single waves, leading depression or leading elevation N-waves, as well as transient waves are presented in this paper. Such solutions are convenient for obtaining a first assessment of tsunami impact on beaches, and they are also useful for experimental investigations and for the purpose of calibrating runup modules in numerical models. We emphasize, however, that the modelling of real tsunamis and their impact on coastlines require advanced numerical modelling incorporating three-dimensional effects such as refraction and diffraction, but this is beyond the scope of the present work.

Since the early 1970s, the prevailing paradigm has been to assume that solitary or cnoidal waves can be used to model some of the important features of tsunamis

† Email address for correspondence: prm@mek.dtu.dk
‡ Present address: SchäfferWaves, Sortedam Dossering 59 D st., DK-2100 Copenhagen ∅, Denmark. Email address: Hemming@SchafferWaves.dk

https://doi.org/10.1017/S0022112009992485 Published online by Cambridge University Press

approaching the beach, and that these theories, originating from the KdV equation, can define the relevant input waves for physical and mathematical models of tsunamis and their associated processes. In the solitary wave paradigm the incoming wave is typically given on the form

$$\eta(x,t) = H\,\mathrm{sech}^2\left(K_s(x-ct)\right), \quad K_s = \frac{1}{h}\sqrt{\frac{3H}{4h}}, \tag{1.1}$$

i.e. the wavenumber is defined by the ratio of the wave height to the water depth. The theoretical work by Synolakis (1987) represents an important milestone by deriving analytical runup formulas for incoming solitary waves. Examples from the literature utilizing and promoting this paradigm are numerous (see e.g. Goring 1978; Synolakis & Deb 1988; Synolakis, Deb & Skjelbreia 1988; Yeh *et al.* 1994; Briggs *et al.* 1995; Liu *et al.* 1995; Li & Raichlen 2001, 2002, 2003; Tonkin *et al.* 2003; Jensen, Pedersen & Wood 2003; Synolakis & Bernard 2006; Lynett *et al.* 2008).

As an alternative to this paradigm, Tadepalli & Synolakis (1994) introduced the concept of N-waves, which were defined as e.g. *isosceles N-waves* given by

$$\eta(x,0) = \frac{3\sqrt{3}}{2}H\,\mathrm{sech}^2\left(K_{is}(x-x_1)\right)\tanh\left(K_{is}(x-x_1)\right), \quad K_{is} = \frac{3}{2h}\sqrt{\frac{H}{h}\sqrt{\frac{3}{4}}} \tag{1.2}$$

or *generalized N-waves* given by

$$\eta(x,0) = \alpha\frac{H}{h}(x-x_2)\,\mathrm{sech}^2\left(K_s(x-x_1)\right), \quad K_s = \frac{1}{h}\sqrt{\frac{3H}{4h}} \tag{1.3}$$

with α being a scaling parameter (of order one) included to ensure that the wave height of the N-wave was actually H. To a certain degree, the work by Tadepalli & Synolakis (1994) represented a change from the solitary wave paradigm (see the reviews by Synolakis, Okal & Bernard 2005; Synolakis & Bernard 2006). However, first of all, their work did not have much impact on procedures used in experimental studies of tsunamis. Secondly, the N-wave expressions (such as (1.2)–(1.3)) both incorporate the classical solitary wave tie between the wavenumber K_s and the nonlinearity H/h, which means that they are basically composed of solitary or solitary-like waves.

Recently, Madsen, Fuhrman & Schäffer (2008) demonstrated that waves incorporating the solitary wave tie are fundamentally inappropriate for geophysical tsunamis, and they came to the following conclusions:

(a) Initial surface displacements due to seismic activity in the deep ocean tend to develop leading waves governed by weak linear dispersion. Hence during this stage, the appropriate model is the linear KdV equation for which the solution is a convolution involving the initial elevation and the Airy function. With time the effective dispersion associated with the leading waves will decrease, and at some stage it will reach the level of nonlinearity at hand. In principle, this heralds a shift to the full KdV dynamics, but it will not occur within realistic travel distances in the ocean or on the continental shelf.

(b) During shoaling from the deep ocean to the nearshore, nonlinearity grows rapidly, while the effect of dispersion becomes smaller and smaller. In this process, the asymmetry of the wave profiles will increase, while skewness remains at low levels and representative wave periods in the transient wave stay almost constant even on very mild bottom slopes. During this stage the appropriate model is the nonlinear shallow-water (NSW) equations.

(c) Close to the beach the front face of the tsunami may become rather steep, and in this case it can disintegrate into an undular bore with short and steep transient

https://doi.org/10.1017/S0022112009992485 Published online by Cambridge University Press

waves. These are typically of the order 10–15 s events riding on top of the main tsunami, which may be of the order 5–30 min. As demonstrated by Madsen *et al.* (2008), the very short waves in the front of the tsunami do represent the KdV scale, and such events have indeed been observed on several occasions. However, it is misleading to focus on these short waves in the undular bore without addressing the main flood wave.

(d) Tsunamis are sometimes reported to be breaking close to the beach. However, it is typically the short waves riding on top of the tsunami which are breaking rather than the main tsunami itself, and therefore the runup will not necessarily be strongly influenced by this breaking process.

On the basis of the work by Madsen *et al.* (2008), we can conclude that from its generation in the ocean to its impact at the shore, the relevant length- and time-scales of the bulk tsunami is never defined by the solitary wave tie i.e. given by the ratio of the wave height to the water depth. This questions the geophysical relevance of earlier analytical and experimental work on the runup of breaking or non-breaking relatively short solitary waves such as reported by, e.g. Synolakis (1987), Briggs *et al.* (1995), Liu *et al.* (1995), Li & Raichlen (2001, 2002, 2003), Tonkin *et al.* (2003), Jensen *et al.* (2003) and Lynett *et al.* (2008). Obviously, it makes a difference whether you consider the runup of wind waves, tsunamis or tidal waves. The solitary waves used as input in so many laboratory tests throughout the last 20 years represent wave phenomena at a completely different time- and space-scale than those associated with tsunamis. The runup and the associated wave breaking are very sensitive to whether the typical wave period is 15 s or 15 min in prototype scale. No matter if full scale tsunami phenomena or their laboratory model scale equivalents are considered, it is inappropriate to use the prevailing solitary wave tie to link the ratio of the vertical scale (wave height) to the horizontal scale (wavelength or equivalently the period).

To be fair to the work by Tadepalli & Synolakis (1994), it should be mentioned that Geist & Yoshioka (1996) were actually able to use their generalized N-wave formulation (1.3) as a match of computed tsunami wave forms along the continental shelf (depth 1 km) in connection with the Cascadia faults (see their figure 14). However, unfortunately, they did not provide sufficient information about how they succeeded to break loose from the solitary wave tie and match the geophysical length scales with (1.3). A recent personal communication with Eric Geist has revealed some of the mystery: After realizing that the conventional use of (1.3) would fail, he calibrated H/h to match the horizontal length scale of the phenomenon (via K_s). This would make H/h orders of magnitude different from the physical value, but he then calibrated α to twist the wave height back in place. For the five cases shown in figure 14 in Geist & Yoshioka (1996), the following calibration parameters were applied: (*a*) $H/h = 0.007$, $\alpha = -0.0148$; (*b*) $H/h = 0.035$, $\alpha = -0.0061$; (*c*) $H/h = 0.049$, $\alpha = -0.0087$; (*d*) $H/h = 0.019$, $\alpha = 0.00255$; (*e*) $H/h = 0.027$, $\alpha = -0.0090$. The actual wave height-to-depth ratios were much smaller than these values. Hence, we do acknowledge, that the expressions derived by Tadepalli & Synolakis (1994) can be applied to geophysical events if the parameters are tweaked accordingly. Furthermore, it should be mentioned that Tadepalli & Synolakis (1996) modified their original formulation (1.3) to incorporate an extra free parameter p_0 in the determination of the wavenumber

$$K_s = \frac{1}{h}\sqrt{p_0 \frac{3H}{4h}}. \tag{1.4}$$

However, they did not discuss why this was necessary and they did not provide any guidance in choosing the parameters. In the examples presented by Tadepalli

https://doi.org/10.1017/S0022112009992485 Published online by Cambridge University Press

& Synolakis (1996), p_0 was either set to unity (their figure 1) or it was undefined (their figures 2, 3, 4 and 5). One of the reviewers of the present paper has now kindly provided a set of parameters leading to a good match of the incoming wave profile of the Nicaragua 1992 tsunami shown in Tadepalli & Synolakis (1996), their figure 5: The water depth was $h = 3000$ m, and the parameters in (1.3)–(1.4) were chosen to be $H/h = 0.00033$, $\alpha = 0.43394$, $x_1/h = 17$, $x_2/h = 16.5$ and $p_0 = 200$ leading to $K_s h = 0.2225$. The fact that p_0 is so large (and not of order unity as expected), actually confirms our viewpoint that the solitary wave tie for tsunamis is a flaw. We have not been able to find any previous papers that discuss the necessity of fixing this problem or address when and how this could and should be done.

In this work, we first derive analytical solutions for the runup/rundown of incoming single waves described by $\mathrm{sech}^2(\Omega t - Kx)$, where Ω is chosen freely rather than being tied to the wave height to depth ratio as in solitary wave theory. Furthermore, we consider incoming leading depression waves composed of a superposition of positive and negative single waves. Finally, we present a simple and fast method to evaluate the runup of incoming transient wavetrains. The work is organized as follows. Section 2.1 gives a brief summary of the linear runup solution by Keller & Keller (1964) for the canonical problem of a constant depth section attached to a constant slope section. Section 2.2 provides a brief review of the hodograph transformation for nonlinear waves by Carrier & Greenspan (1958), and discusses the corresponding breaking criterion. In §§ 2.3–2.4, general expressions for the runup elevation and the associated velocity are given in terms of inverse Fourier transforms involving the time series of the incoming wavetrain at the foot of the slope. These transforms can be determined either by complex contour integration or by convolution integrals. The former method is well suited for providing analytical expressions for simple wave forms, while the latter is particularly useful for arbitrary input wavetrains. These solutions are developed for sinusoidal waves in § 3 and for single waves in § 4. By applying the classical solitary wave tie between the duration and the nonlinearity, we recover the solution by Synolakis (1987) for solitary waves. Section 5 deals with leading depression N-waves composed of a superposition of positive and negative single waves. In § 6, the maximum runup solutions are combined with the theoretical breaking criteria, and the results for sinusoidal waves, single waves and leading depression waves are discussed in the framework of the surf similarity parameter. Finally, in § 7, we consider incoming transient wavetrains generated by monopole and dipole disturbances in the deep ocean. The evolution of these wavetrains, while travelling over constant depth in the deep ocean is described by a convolution integral involving the Airy function, and the runup on the plane sloping beach is then determined by another convolution integral involving the incoming surface elevation time series at the foot of the slope. Summary and conclusions are given in § 8.

2. Governing equations for the runup of nonlinear long waves

Theoretical analyses of long wave runup on beaches are usually based on either the linear or the NSW equations. While the linear solutions go back a long time (see e.g. Green 1838; Lamb 1932; Lewy 1946), Carrier & Greenspan (1958) were the first to provide an analytical solution to the NSW equations for the runup of normally incident monochromatic waves on a uniformly sloping beach. Later, Carrier (1971) and Synolakis (1987) came to the important conclusion that the maximum runup on the beach evaluated from linear theory is identical to the one evaluated from nonlinear theory, despite the fact that the solutions in general may deviate

https://doi.org/10.1017/S0022112009992485 Published online by Cambridge University Press

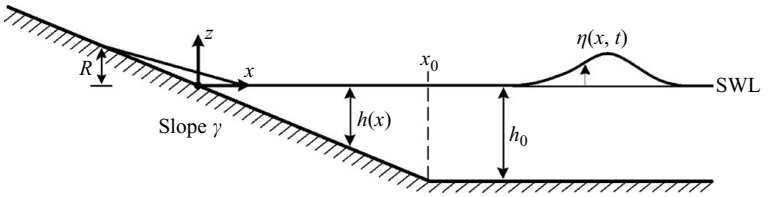


FIGURE 1. A definition sketch for a single wave climbing up a sloping beach. Still water level (SWL).

significantly in time and space. Keller & Keller (1964) were the first to consider the canonical problem of waves propagating first over a constant depth offshore region and then up a uniformly sloping beach. They provided a linear solution to this problem for sinusoidal incident waves. Later, their work was extended to waves of different forms by, e.g. Gjevik & Pedersen (1981), Synolakis (1987), Synolakis & Deb (1988), Synolakis *et al.* (1988), Pelinovsky & Mazova (1992), Tadepalli & Synolakis (1994, 1996), Li & Raichlen (2001), Didenkulova *et al.* (2006), and Didenkulova *et al.* (2007). Most of these extensions utilize a combination of Carrier and Greenspan's nonlinear hodograph transformation (Carrier & Greenspan 1958) and Keller and Keller's linear transfer function (Keller & Keller 1964) from the flat bottom to the slope.

In this work we follow the derivation procedure outlined by Synolakis (1987). The one-dimensional bathymetry consists of an offshore constant depth region attached to a plane sloping beach (see figure 1). The coordinate system has its origin at the still water shoreline, with the x-axis pointing in the offshore direction and the z-axis pointing upwards. Hence, the spatial variation of the still water depth is described by $h(x) = \gamma x$, for $x \leqslant x_0$, and $h(x) = h_0$, for $x \geqslant x_0$, with γ being the constant beach slope. A boundary value problem (BVP) is considered, and the objective is to establish the runup in terms of the incoming time series at the foot of the slope. The incoming waves are assumed to obey the linear shallow-water equations or the linear KdV equation in the constant depth region, while they obey the NSW equations on the sloping beach. Throughout this paper, the effects of wave breaking and bottom dissipation are neglected, and full reflection from the beach is assumed.

2.1. *The linear sinusoidal wave solution*

In the following we briefly summarize the linear solution to the BVP problem sketched above as first derived by Keller & Keller (1964). The incoming and reflected waves propagating over the flat bottom are described as linear sinusoidal long waves with amplitudes A_i and A_r. With full reflection at the shoreline the linear standing wave solution on the sloping beach becomes

$$\eta_s(x, t) = A_s J_0(\sigma) \mathrm{e}^{-\mathrm{i}\omega t}, \qquad U_s(x, t) = \mathrm{i}\frac{2\omega}{\gamma} A_s \frac{J_1(\sigma)}{\sigma} \mathrm{e}^{-\mathrm{i}\omega t}, \tag{2.1}$$

where $\eta_s(x, t)$ is the surface elevation and $U_s(x, t)$ the velocity component in the x direction. Furthermore, A_s is the shoreline elevation amplitude, J_n is the nth-order Bessel function of the first kind, i is the imaginary unit and ω is the angular frequency. Finally, σ is defined by

$$\sigma \equiv 2\omega \sqrt{\frac{x}{g\gamma}}, \tag{2.2}$$

https://doi.org/10.1017/S0022112009992485 Published online by Cambridge University Press

where g is the acceleration of gravity. At the toe of the slope we have $x_0 = h_0/\gamma$, i.e.

$$\sigma_0 = 2\omega t_0 = 2k_0 x_0, \quad \text{where} \quad t_0 \equiv \frac{x_0}{\sqrt{gh_0}}, \quad k_0 \equiv \frac{\omega}{\sqrt{gh_0}}. \tag{2.3}$$

Continuity in surface elevation and velocity at $x = x_0$ now leads to the solution

$$A_r = \left(\frac{J_0(\sigma_0) + \mathrm{i}J_1(\sigma_0)}{J_0(\sigma_0) - \mathrm{i}J_1(\sigma_0)}\right) A_i \mathrm{e}^{-\mathrm{i}2k_0 x_0}, \qquad A_s = \left(\frac{2}{J_0(\sigma_0) - \mathrm{i}J_1(\sigma_0)}\right) A_i \mathrm{e}^{-\mathrm{i}k_0 x_0}, \tag{2.4}$$

and by inserting (2.4) into (2.1) we obtain

$$\eta_s(x,t) = \left(\frac{2J_0(\sigma)}{J_0(\sigma_0) - \mathrm{i}J_1(\sigma_0)}\right) \eta_i(x_0,t), \tag{2.5}$$

which determines the surface elevation on the sloping beach in terms of the time series of the incoming wave at $x = x_0$. Although this result is restricted to linear sinusoidal waves, Synolakis (1987) demonstrated its importance for establishing nonlinear solutions for more general wave forms. We shall discuss this issue in further detail in the following sections.

2.2. *The hodograph transformation by Carrier & Greenspan (1958)*

We now return to the problem of nonlinear waves on the sloping beach described by the NSW equations. The conventional form of these equations reads

$$\frac{\partial \eta}{\partial t} + \frac{\partial}{\partial x}(U(h+\eta)) = 0, \qquad \frac{\partial U}{\partial t} + U\frac{\partial U}{\partial x} + g\frac{\partial \eta}{\partial x} = 0. \tag{2.6}$$

It is by no means a trivial task to obtain analytical solutions to these equations, but Carrier & Greenspan (1958) provided an elegant method in their pioneering work, which we briefly summarize in the following. Firstly, (2.6) is expressed in characteristic form by which the Riemann invariants (α, β) are identified. Secondly, the independent coordinates are transformed from (x, y) to (α, β), which leads to

$$\frac{\partial x}{\partial \alpha} - (U - C)\frac{\partial t}{\partial \alpha} = 0, \qquad \frac{\partial x}{\partial \beta} - (U + C)\frac{\partial t}{\partial \beta} = 0, \tag{2.7}$$

where

$$\alpha \equiv U + 2C - g\gamma t, \qquad \beta \equiv U - 2C - g\gamma t, \qquad C \equiv \sqrt{g(h+\eta)}. \tag{2.8}$$

Thirdly, a new set of independent variables (ρ, λ) is introduced in terms of the sum and difference of the (α, β) variables. Many slightly different formulations of this step has been reported in the literature (see e.g. Carrier & Greenspan 1958; Synolakis 1987; Mei, Yue & Stiassnie 2005), but we prefer a formulation where λ becomes equal to t in the linear limit. This is achieved by using

$$\lambda \equiv -\frac{1}{2g\gamma}(\alpha + \beta), \qquad \rho \equiv \frac{1}{2g\gamma}(\alpha - \beta). \tag{2.9}$$

Furthermore, we introduce the velocity potential $\psi(\rho, \lambda)$ defined by

$$\frac{\partial \psi}{\partial \rho} = \rho U, \qquad \frac{\partial \psi}{\partial \lambda} = 2\left(x - \frac{U^2}{2g\gamma} - \frac{g\gamma\rho^2}{4}\right). \tag{2.10}$$

When (2.9) and (2.10) are inserted into (2.7), the following linear differential equation is obtained

$$\frac{\partial^2 \psi}{\partial \rho^2} + \frac{1}{\rho}\frac{\partial \psi}{\partial \rho} - \frac{\partial^2 \psi}{\partial \lambda^2} = 0. \tag{2.11}$$

https://doi.org/10.1017/S0022112009992485 Published online by Cambridge University Press

This is the main achievement of using the hodograph technique: The fact that two nonlinear equations in physical space can be expressed as a single linear equation in transformed space.

The remaining step is to express η, U, x and t in terms of ψ, ρ and λ and from (2.8)–(2.10) the following relations can be obtained

$$U(\rho,\lambda)=\frac{1}{\rho}\frac{\partial\psi}{\partial\rho},\qquad \eta(\rho,\lambda)=-\left(\frac{\gamma}{2}\frac{\partial\psi}{\partial\lambda}+\frac{U^2}{2g}\right), \tag{2.12}$$

$$t(\rho,\lambda)=\lambda+\frac{U}{g\gamma},\qquad x(\rho,\lambda)=\frac{1}{2}\frac{\partial\psi}{\partial\lambda}+\frac{U^2}{2g\gamma}+\frac{g\gamma\rho^2}{4}. \tag{2.13}$$

We note that the mapping between (x,t) and (ρ,λ) is governed by the chain rule, e.g.

$$\frac{\partial\eta}{\partial\lambda}=\frac{\partial\eta}{\partial x}\frac{\partial x}{\partial\lambda}+\frac{\partial\eta}{\partial t}\frac{\partial t}{\partial\lambda},\qquad \frac{\partial\eta}{\partial\rho}=\frac{\partial\eta}{\partial x}\frac{\partial x}{\partial\rho}+\frac{\partial\eta}{\partial t}\frac{\partial t}{\partial\rho}, \tag{2.14}$$

which leads to

$$\frac{\partial\eta}{\partial x}=\frac{M_1}{M_0},\qquad \frac{\partial\eta}{\partial t}=\frac{M_2}{M_0}, \tag{2.15}$$

where

$$M_0\equiv\begin{vmatrix}\frac{\partial x}{\partial\rho} & \frac{\partial t}{\partial\rho}\\ \frac{\partial x}{\partial\lambda} & \frac{\partial t}{\partial\lambda}\end{vmatrix},\qquad M_1\equiv\begin{vmatrix}\frac{\partial\eta}{\partial\rho} & \frac{\partial t}{\partial\rho}\\ \frac{\partial\eta}{\partial\lambda} & \frac{\partial t}{\partial\lambda}\end{vmatrix},\qquad M_2\equiv\begin{vmatrix}\frac{\partial x}{\partial\rho} & \frac{\partial\eta}{\partial\rho}\\ \frac{\partial x}{\partial\lambda} & \frac{\partial\eta}{\partial\lambda}\end{vmatrix} \tag{2.16}$$

and equivalent expressions for the derivatives of U. In this process the ρ and λ derivatives of x, t, η and U are easily determined by (2.12)–(2.13), and in combination with (2.11) this leads to, e.g.

$$M_0=\frac{\rho}{2g\gamma}\left(\left(g\gamma+\frac{\partial U}{\partial\lambda}\right)^2-\left(\frac{\partial U}{\partial\rho}\right)^2\right). \tag{2.17}$$

Obviously, the Jacobian M_0 plays an important role in this mapping.

2.2.1. *Conditions at the shoreline*

The moving shoreline is defined where $d=h+\eta$ is zero at all time. According to (2.8), this implies that C should be zero, which in turn according to (2.9) implies that this location is defined by $\rho=0$. The runup elevation R and the associated runup velocity V are defined by

$$R(\lambda)=\lim_{\rho\to0}\eta(\rho,\lambda),\qquad V(\lambda)=\lim_{\rho\to0}U(\rho,\lambda). \tag{2.18}$$

It turns out that simple relations can be established for the time derivatives of R and V despite the nonlinear transformation: As both quantities are associated to the shoreline, which is moving in (x,t) space, it follows that

$$\frac{\mathrm{d}R}{\mathrm{d}t}=\lim_{\rho\to0}\left(\frac{\partial\eta}{\partial t}+U\frac{\partial\eta}{\partial x}\right),\qquad \frac{\mathrm{d}V}{\mathrm{d}t}=\lim_{\rho\to0}\left(\frac{\partial U}{\partial t}+U\frac{\partial U}{\partial x}\right). \tag{2.19}$$

Firstly, we insert (2.15) and the equivalent expressions for the derivatives of U in (2.19). Secondly, we perform a Taylor expansion of (2.19) around $\rho=0$, and this is achieved by considering a general solution of the form $\psi\sim J_0(\omega\rho)F(\omega\lambda)$, where F is

https://doi.org/10.1017/S0022112009992485 Published online by Cambridge University Press

an unknown function. This effort leads to

$$\frac{\mathrm{d}R}{\mathrm{d}t} = -\gamma V(t), \qquad \frac{\mathrm{d}V}{\mathrm{d}t} = \frac{\mathrm{d}V}{\mathrm{d}\lambda}\left(1 + \frac{1}{g\gamma}\frac{\mathrm{d}V}{\mathrm{d}\lambda}\right)^{-1}, \tag{2.20}$$

and

$$\lim_{\rho\to 0}\left(\frac{\partial \eta}{\partial x}\right) = -\frac{1}{g}\frac{\mathrm{d}V}{\mathrm{d}t}. \tag{2.21}$$

Notice how (2.20)–(2.21) provide a simple relation between the derivatives of R, V and η despite the fact that they are solutions to the NSW equations at the moving shoreline.

2.2.2. *Theoretical breaking criterion*

While the velocity potential ψ, which satisfies (2.11) is always a single-valued function of ρ and λ, it may become multi-valued in terms of x and t. This happens if the Jacobian M_0 becomes zero inside the fluid domain, i.e. for $\rho > 0$, and in this case the mapping formally breaks down. This defines a theoretical breaking criterion for the solutions. We notice from (2.17) that in fact M_0 always vanishes at the instantaneous shoreline ($\rho = 0$), and check if M_0/ρ can vanish in the vicinity of the shoreline, i.e. for $\rho \to 0$. To identify this situation, we again assume a general solution of the form $\psi \sim J_0(\omega\rho)F(\omega\lambda)$, where F is an unknown function, and expand M_0 around $\rho = 0$. This leads to

$$\left(g\gamma + \frac{\partial U}{\partial \lambda}\right)^2 = O\left(1\right), \quad \text{and} \quad \left(\frac{\partial U}{\partial \rho}\right)^2 = O\left(\rho^2\right), \tag{2.22}$$

and allows us to ignore the last term in (2.17) for $\rho \to 0$. Hence we obtain the following theoretical breaking criterion in the vicinity of the shoreline:

$$\frac{1}{g\gamma}\frac{\partial U}{\partial \lambda} \to -1 \quad \text{for } \rho \to 0. \tag{2.23}$$

Note that according to (2.20)–(2.21), this criterion will make the t derivative of V and the x derivative of η go to infinity, corresponding to a vertical front face in these profiles.

This completes the description of the hodograph procedure first developed by Carrier & Greenspan (1958). As we have used slightly different definitions of the (ρ, λ) variables and of the velocity potential ψ, the various relations between ρ, λ, ψ in transformed space and x, t, U and η in physical space differ from the ones of Carrier & Greenspan (1958), Gjevik & Pedersen (1981), Synolakis (1987), Mei *et al.* (2005) and Carrier, Wu & Yeh (2003).

2.3. *The runup formulation in terms of inverse Fourier transforms*

The objective in this section is to express solutions to (2.11) in terms of Fourier transforms. The Fourier transform of ψ (with respect to λ) and the corresponding inverse Fourier transform are defined by

$$\widetilde{\psi}(\rho,\omega) = \frac{1}{\sqrt{2\pi}}\int_{-\infty}^{\infty}\psi(\rho,\lambda)\mathrm{e}^{\mathrm{i}\omega\lambda}\,\mathrm{d}\lambda, \quad \psi(\rho,\lambda) = \frac{1}{\sqrt{2\pi}}\int_{-\infty}^{\infty}\widetilde{\psi}(\rho,\omega)\mathrm{e}^{-\mathrm{i}\omega\lambda}\,\mathrm{d}\omega. \tag{2.24}$$

Now, the Fourier transform of each of the terms in the governing equation (2.11) yields

$$\frac{\partial^2\widetilde{\psi}}{\partial\rho^2} + \frac{1}{\rho}\frac{\partial\widetilde{\psi}}{\partial\rho} + \omega^2\widetilde{\psi} = 0,$$

https://doi.org/10.1017/S0022112009992485 Published online by Cambridge University Press

which has the solution

$$\widetilde{\psi}(\rho, \omega) = B J_0(\omega\rho), \tag{2.25}$$

where J_0 is the zeroth order Bessel function of the first kind and B is a complex coefficient.

In order to determine B, boundary conditions at the toe of the slope ($x = x_0$) should be established. In general, this location is not well defined in ρ space, because of the nonlinear relation (2.13) between x and ρ. Synolakis (1987) resolved this problem by assuming that the toe of the slope is so far away from the shoreline that the nonlinear effects in the coordinate transformation can be ignored. In this case (2.9) simplify to

$$\lambda \simeq t, \quad \rho_0 \simeq 2\sqrt{\frac{x_0}{g\gamma}}, \tag{2.26}$$

i.e. the linearization makes λ equal to t, while ρ_0 becomes proportional to $\sqrt{x_0}$. Furthermore, we notice from (2.3) that the linearization leads to $\omega\rho_0 \simeq \sigma_0 = 2\omega t_0$.

Naturally, the linearization of the coordinate transformation is a limitation of the method, if we want to allow for nonlinear waves at the toe of the slope, and in this respect it was somewhat paradoxical that Synolakis (1987) and Synolakis *et al.* (1988) used this approach to study the runup of incoming finite amplitude cnoidal and solitary waves. Li & Raichlen (2002) improved the matching procedure for weakly nonlinear waves and considered incoming solitary waves with height over depth ratios H/h_0 from 0.1 to 0.5. They found that their correction was important for $H/h_0 > 0.15$. However, for seismic tsunamis generated in the deep ocean, the linearization of offshore wave conditions and coordinate transformations is legitimate. Consequently, we can also linearize (2.12) at the toe of the slope to obtain

$$\eta(\rho_0, \lambda) \simeq -\frac{\gamma}{2}\frac{\partial\psi}{\partial\lambda}, \tag{2.27}$$

and in combination with (2.25) this yields

$$\widetilde{\psi}(\rho, \omega) = -\frac{2\mathrm{i}}{\omega\gamma}\frac{J_0(\omega\rho)}{J_0(\omega\rho_0)}\widetilde{\eta}(\rho_0, \omega). \tag{2.28}$$

We have now expressed the general solution $\widetilde{\psi}(\rho, \omega)$ in terms of the boundary condition $\widetilde{\eta}(\rho_0, \omega)$, which defines the Fourier transform of the standing wave solution at the toe of the slope. As we assume that the wave conditions are linear at this location, we can utilize Keller and Keller's (Keller & Keller 1964) linear solution (2.5) with $x = x_0$. This leads to

$$\widetilde{\eta}(\rho_0, \omega) = \widetilde{\Phi}_i(\omega)\left(\frac{2J_0(\sigma_0)}{J_0(\sigma_0) - \mathrm{i}J_1(\sigma_0)}\right), \tag{2.29}$$

where

$$\widetilde{\Phi}_i(\omega) \equiv \frac{1}{\sqrt{2\pi}}\int_{-\infty}^{\infty}\Phi_i(t)\mathrm{e}^{\mathrm{i}\omega t}\,\mathrm{d}t, \qquad \Phi_i(t) \equiv \eta_i(x_0, t). \tag{2.30}$$

By inserting (2.29) in (2.28), utilizing that $\omega\rho_0 \simeq \sigma_0 = 2\omega t_0$, and taking the inverse Fourier transform, we now obtain

$$\psi(\rho, \lambda) = -\frac{4\mathrm{i}}{\gamma\sqrt{2\pi}}\int_{-\infty}^{\infty}\frac{\widetilde{\Phi}_i(\omega)}{\omega}\left(\frac{J_0(\omega\rho)}{J_0(2\omega t_0) - \mathrm{i}J_1(2\omega t_0)}\right)\mathrm{e}^{-\mathrm{i}\omega\lambda}\,\mathrm{d}\omega. \tag{2.31}$$

https://doi.org/10.1017/S0022112009992485 Published online by Cambridge University Press

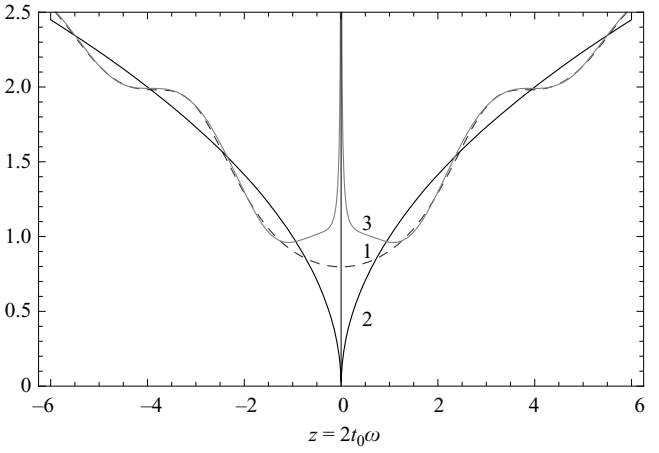


FIGURE 2. The absolute value of the Bessel-transfer function $\widetilde{\Psi}_\eta$ versus its asymptotic approximations for large arguments. (1) Left hand side of (2.35); (2) first approximation truncated at $O(z^{-1/2})$; (3) second approximation truncated at $O(z^{-3/2})$.

Next, we determine $\eta(\rho, \lambda)$ and $U(\rho, \lambda)$ on the basis of (2.12) and (2.31), and by letting $\rho \to 0$ in these expressions we obtain the shoreline motions

$$V(\lambda) \equiv \lim_{\rho\to 0} U = -\frac{1}{\gamma}\int_{-\infty}^{\infty} \widetilde{\Psi}_u(\omega)\widetilde{\Phi}_i(\omega)\mathrm{e}^{-\mathrm{i}\omega\lambda}\,\mathrm{d}\omega, \tag{2.32}$$

$$R(\lambda) \equiv \lim_{\rho\to 0} \eta = \int_{-\infty}^{\infty} \widetilde{\Psi}_\eta(\omega)\widetilde{\Phi}_i(\omega)\mathrm{e}^{-\mathrm{i}\omega\lambda}\,\mathrm{d}\omega - \frac{V^2}{2g}, \tag{2.33}$$

where

$$\widetilde{\Psi}_\eta(\omega) \equiv \frac{2}{\sqrt{2\pi}}\left(\frac{1}{J_0(2\omega t_0) - \mathrm{i}J_1(2\omega t_0)}\right), \qquad \widetilde{\Psi}_u(\omega) \equiv -\mathrm{i}\omega\widetilde{\Psi}_\eta(\omega). \tag{2.34}$$

It turns out that this expression for $\widetilde{\Psi}_\eta(\omega)$ has some disadvantages: First of all, it prevents us from obtaining closed form analytical solutions to (2.33)–(2.33), e.g. in connection with complex contour integration. Secondly, we have not been able to determine its inverse Fourier transform $\Psi_\eta(\lambda)$, which is necessary for the convolution approach discussed in the following section. However for large arguments of the Bessel functions we may use the approximation

$$\frac{2}{\sqrt{2\pi}}\left(\frac{1}{J_0(z) - \mathrm{i}J_1(z)}\right) \to (-\mathrm{i}z)^{1/2}\mathrm{e}^{\mathrm{i}z} + (-\mathrm{i}z)^{-1/2}\left(\frac{1}{8}\mathrm{e}^{\mathrm{i}z} - \frac{1}{4}\mathrm{sign}(z)\mathrm{e}^{\mathrm{i}3z}\right) + O(z^{-3/2}). \tag{2.35}$$

Figure 2 shows a comparison between the absolute values of the general expression and the approximations truncated either at $O(z^{-1/2})$ or at $O(z^{-3/2})$. The general expression starts at $\sqrt{2/\pi}$ for $z = 0$ and slowly oscillates while growing for larger values of z. In contrast, the approximation truncated at $O(z^{-1/2})$ starts at zero for $z = 0$ and grows without oscillations, while the approximation truncated at $O(z^{-3/2})$ starts at infinity but quickly attaches to the general expression with a similar oscillatory pattern. However, the singularity at $z = 0$, makes the approximation truncated at $O(z^{-3/2})$ less attractive, and instead we concentrate on the approximation truncated at $O(z^{-1/2})$. In this case the relative error is less than 5 % for $z = 2t_0\omega > 4.88$, which according to (2.3) corresponds to $x_0/L_0 > 0.4$, where $L_0 = T\sqrt{gh_0}$.

https://doi.org/10.1017/S0022112009992485 Published online by Cambridge University Press

This approximation, which was also used by, e.g. Synolakis (1987) and Tadepalli & Synolakis (1994), leads to

$$\widetilde{\Psi}_\eta(\omega) \simeq (-\mathrm{i}\omega)^{1/2}\sqrt{2t_0}\,\mathrm{e}^{\mathrm{i}2t_0\omega}, \quad \widetilde{\Psi}_u(\omega) \simeq (-\mathrm{i}\omega)^{3/2}\sqrt{2t_0}\,\mathrm{e}^{\mathrm{i}2t_0\omega}. \tag{2.36}$$

We substitute (2.36) into (2.33)–(2.33) and obtain

$$V(\lambda) = -\frac{\sqrt{2t_0}}{\gamma}\int_{-\infty}^{\infty}(-\mathrm{i}\omega)^{3/2}\widetilde{\Phi}_i(\omega)\mathrm{e}^{-\mathrm{i}\omega(\lambda-2t_0)}\,\mathrm{d}\omega, \tag{2.37}$$

$$R(\lambda) = \sqrt{2t_0}\int_{-\infty}^{\infty}(-\mathrm{i}\omega)^{1/2}\widetilde{\Phi}_i(\omega)\mathrm{e}^{-\mathrm{i}\omega(\lambda-2t_0)}\,\mathrm{d}\omega - \frac{V^2}{2g}. \tag{2.38}$$

Notice that both expressions belong to the family of *fractional derivatives*: The runup elevation is essentially the *half-derivative* of the time series at the foot of the slope, while the runup velocity is essentially the *three-halves derivative*. The factor $\mathrm{e}^{\mathrm{i}2t_0\omega}$ represents a delay in the runup signal of $2t_0$, which is caused by the travelling time over the sloping beach, i.e.

$$\int_0^{x_0}\frac{\mathrm{d}x}{c} = \int_0^{x_0}\frac{\mathrm{d}x}{\sqrt{g\gamma x}} = 2t_0.$$

Generally, there are two ways to solve (2.38)–(2.38): As a first approach, we may determine the inverse Fourier transform e.g. by complex contour integration, which is convenient in case $\widetilde{\Phi}_i$ has simple poles in the complex plane (see e.g. Synolakis 1987). The advantage of this approach is that it will lead to analytical expressions for the runup. As a second approach, we may apply the convolution theorem, which is discussed in the following section.

2.4. *The runup formulation in terms of convolution integrals*

According to the convolution theorem the inverse Fourier transform of the product $\widetilde{\Psi}\widetilde{\Phi}_i$ can be replaced by the convolution between Ψ and Φ_i, i.e.

$$\int_{-\infty}^{\infty}\widetilde{\Psi}(\omega)\widetilde{\Phi}_i(\omega)\mathrm{e}^{-\mathrm{i}\omega\lambda}\mathrm{d}\omega = \int_{-\infty}^{\infty}\Psi(s)\Phi_i(\lambda-s)\,\mathrm{d}s. \tag{2.39}$$

This calls for analytical expressions for the inverse Fourier transforms of $\widetilde{\Psi}_\eta$ and $\widetilde{\Psi}_u$, which are straightforward to determine from (2.36). As an alternative, however, we introduce the impulse response function

$$G(\lambda) \equiv \frac{1}{\sqrt{2\pi}}\int_{-\infty}^{\infty}\frac{\widetilde{\Psi}_\eta}{(-\mathrm{i}\omega)}\mathrm{e}^{-\mathrm{i}\omega\lambda}\,\mathrm{d}\omega = \frac{1}{\sqrt{2\pi}}\int_{-\infty}^{\infty}\frac{\widetilde{\Psi}_u}{(-\mathrm{i}\omega)^2}\mathrm{e}^{-\mathrm{i}\omega\lambda}\,\mathrm{d}\omega, \tag{2.40}$$

and in combination with (2.36) this becomes

$$G(\lambda) = \begin{cases} 2\sqrt{t_0}(\lambda-2t_0)^{-1/2}, & \lambda > 2t_0, \\ 0, & \lambda < 2t_0. \end{cases} \tag{2.41}$$

The physical interpretation of this result is that nothing happens at the shoreline until after a delay of $2t_0$ representing the travel time over the sloping beach. Now (2.38)–(2.38) can be replaced by the convolution integrals

$$V(\lambda) = -\frac{1}{\gamma}\int_{2t_0}^{\lambda}G(s)F_u(\lambda-s)\,\mathrm{d}s, \qquad \text{where} \qquad F_u(t) \equiv \frac{\partial^2\Phi_i}{\partial t^2}, \tag{2.42}$$

$$\eta(\lambda) = \int_{2t_0}^{\lambda}G(s)F_\eta(\lambda-s)\,\mathrm{d}s - \frac{V(\lambda)^2}{2g}, \qquad \text{where} \qquad F_\eta(t) \equiv \frac{\partial\Phi_i}{\partial t}. \tag{2.43}$$

https://doi.org/10.1017/S0022112009992485 Published online by Cambridge University Press

This convolution approach is attractive and easy to apply numerically for any sufficiently smooth time series of incoming surface elevation. An example of its application is given in § 7, where we consider an incoming transient wavetrain.

3. Runup solution for sinusoidal waves

The runup solution for sinusoidal waves is well established in the literature (see e.g. Carrier & Greenspan 1958; Mei *et al.* 2005), and we use this case to validate the general expressions from the previous section. Now the time series at $x = x_0$ of the incoming wave is described by

$$\eta_i(x_0, t) = A_0 \cos \Omega(t - t_1), \tag{3.1}$$

where Ω is the angular frequency and t_1 is an arbitrary phase shift. The resulting Fourier transform reads

$$\widetilde{\Phi}_i(\omega) = A_0 \sqrt{\frac{\pi}{2}} \left(\mathrm{e}^{\mathrm{i}\Omega t_1} \delta(\omega - \Omega) + \mathrm{e}^{-\mathrm{i}\Omega t_1} \delta(\omega + \Omega) \right), \tag{3.2}$$

where δ is the Dirac delta function. Inserting (3.2) in (2.38)–(2.38) now leads to

$$V(\lambda) = \frac{\Omega R_0}{\gamma} \sin(\theta + \pi/4), \qquad R(\lambda) = R_0 \cos(\theta + \pi/4) - \frac{V(\lambda)^2}{2g}, \tag{3.3}$$

where

$$\frac{R_0}{A_0 \sqrt{\Omega t_0}} = 2\sqrt{\pi}, \qquad \theta \equiv \Omega(\lambda - t_1 - 2t_0). \tag{3.4}$$

Here t_0 is defined by (2.3), while $t(\lambda)$ is given by letting $\rho \to 0$ in (2.13), i.e.

$$t(\lambda) = \lambda + \frac{V(\lambda)}{g\gamma}. \tag{3.5}$$

The maximum runup occurs when $\theta = -\pi/4$ at which time $V(\lambda) \to 0$ and $R(\lambda) \to R_0$. Similarly, the maximum rundown occurs when $\theta = 3\pi/4$ at which time $V(\lambda) \to 0$ and $R(\lambda) \to -R_0$. The maximum runup velocity occurs when $\theta = -3\pi/4$ and yields $V(\lambda) \to -\omega R_0/\gamma$. The temporal variation of $R(t)$ and $V(t)$ can easily be depicted as a parametric plot in terms of $V(\lambda)$, $R(\lambda)$ and $t(\lambda)$.

3.1. *Breaking criterion for sinusoidal waves*

By differentiation of (3.3) with respect to λ we get

$$\frac{\mathrm{d}V}{\mathrm{d}\lambda} = \frac{\Omega^2 R_0}{\gamma} \cos(\theta + \pi/4), \tag{3.6}$$

which attains its maximum negative value for $\theta = 3\pi/4$, i.e. at the time of maximum rundown. At this moment the breaking criterion (2.23) is met for

$$R_0 = \frac{g\gamma^2}{\Omega^2}. \tag{3.7}$$

Inserting (3.4) into (3.7) now yields the breaking criterion

$$\frac{A_0}{h_0} = \frac{1}{2\sqrt{\pi}} \left(\frac{\Omega^2 h_0}{g\gamma^2} \right)^{-5/4}. \tag{3.8}$$

https://doi.org/10.1017/S0022112009992485 Published online by Cambridge University Press

4. Runup solution for single waves

We now consider a single wave approaching the slope from the constant depth region. Such a single wave event may be described in terms of a Gaussian shape (see e.g. Carrier *et al.* 2003) or in terms of a solitary wave (see e.g. Synolakis 1987). However, as discussed in § 1, it is essential to avoid the classical solitary wave tie between the wavenumber (or frequency) and the wave height to depth ratio. Consequently, we choose the functional shape of a solitary wave, but take the freedom of defining the duration and the height of the wave independently. Hence, at $x = x_0$ the incoming time series is described by

$$\eta_i(x_0, t) = A_0 \operatorname{sech}^2 \Omega\,(t - t_1)\,, \tag{4.1}$$

where the frequency Ω defines the effective time-span of the phenomenon, while t_1 is an arbitrary phase shift. A good estimate of the duration of (4.1) is $T = 2\pi/\Omega$ beyond which the function drops below 0.75 % of its peak value.

Note that Didenkulova *et al.* (2007) recently determined the sensitivity of the maximum runup R_{up} to the incoming shape of single pulses. They considered sinusoidal half-waves given by $\cos^n(\pi\zeta)$, soliton-type waves given by $\operatorname{sech}^n(\zeta)$, Lorentzian waves given by $(1+\zeta^2)^{-n}$ and quasi-Gaussian waves given by $\exp(-\zeta^n)$ for different values of n. For each of the wave forms they introduced a measure of the wave duration, e.g. defined by the spatial integral of the elevation normalized by its wave height. Based on (4.1) this yields $T = 2/\Omega$ in contrast to our choice of $T = 2\pi/\Omega$.

The Fourier transform of (4.1) reads

$$\widetilde{\Phi}_i(\omega) = \left(\frac{A_0}{\Omega^2}\sqrt{\frac{\pi}{2}}\right)\frac{\omega \mathrm{e}^{\mathrm{i}\omega t_1}}{\sinh\frac{\pi\omega}{2\Omega}}. \tag{4.2}$$

We insert (4.2) in (2.38)–(2.38) and obtain

$$V(\lambda) = \frac{A_0\sqrt{\pi t_0}}{\gamma\Omega^2}\mathrm{i}\,\mathrm{e}^{-\mathrm{i}\pi/4}\int_{-\infty}^{\infty}\frac{\omega^{5/2}}{\sinh\frac{\pi\omega}{2\Omega}}\mathrm{e}^{-\mathrm{i}\omega(\lambda-t_1-2t_0)}\,\mathrm{d}\omega, \tag{4.3}$$

$$R(\lambda) = \frac{A_0\sqrt{\pi t_0}}{\Omega^2}\mathrm{e}^{-\mathrm{i}\pi/4}\int_{-\infty}^{\infty}\frac{\omega^{3/2}}{\sinh\frac{\pi\omega}{2\Omega}}\mathrm{e}^{-\mathrm{i}\omega(\lambda-t_1-2t_0)}\,\mathrm{d}\omega - \frac{V^2}{2g}. \tag{4.4}$$

4.1. *Evaluation of contour integrals*

The integrals to be evaluated in (4.4)–(4.4) are

$$I_R = \lim_{R\to\infty}\int_{-R}^{R}\frac{\omega^m \mathrm{e}^{-\mathrm{i}\omega(\lambda-t_1-2t_0)}}{\sinh(b\omega)}\,\mathrm{d}\omega, \tag{4.5}$$

where $b = \pi/(2\Omega)$, $m = 3/2$ for $R(\lambda)$ and $m = 5/2$ for $V(\lambda)$. These integrals can be determined by applying classical techniques from mathematical physics and complex analysis (see e.g. Levinson & Redheffer 1970; Mathews & Howell 2001; Kelly 2006). Synolakis (1987) paved the way by outlining the necessary procedure in connection with solitary waves, which leads to integrals similar to (4.5).

As a result of the contour integration, we get

$$I_R = \mathrm{i}^{m+1}2^{m+2}\Omega^{m+1}\Gamma(m, \theta), \tag{4.6}$$

https://doi.org/10.1017/S0022112009992485 Published online by Cambridge University Press

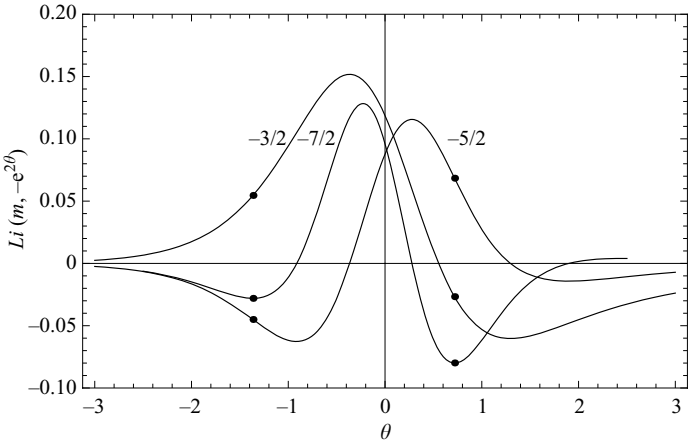


FIGURE 3. Temporal variation of the polylogarithm Li for shoreline motions of a single wave. (a) Elevation polylogarithm ($m=-3/2$); (b) velocity polylogarithm ($m=-5/2$); (c) acceleration polylogarithm ($m=-7/2$). Location of possible breaking shown as markers.

where

$$\Gamma(m,\theta) \equiv \sum_{n=1}^{\infty} (-1)^n n^m \exp(2n\theta), \tag{4.7}$$

$$\theta \equiv \Omega\,(\lambda - t_1 - 2t_0)\,. \tag{4.8}$$

Note that exactly the same phase function was established in (3.4) for the sinusoidal wave input.

The power series (4.8) formally only converges within the open unit disk in the complex plane, i.e. for $|\exp 2\theta| < 1$, but in fact the infinite sum belongs to the so-called *polylogarithm* family Li, which is defined on the whole complex plane via the method of *analytic continuation* (see Lewin 1980 & 1991; Wood 1992; Weisstein 2005). From the general definition of the Li function we identify that

$$\Gamma(m,\theta) = Li\left(-m, -\mathrm{e}^{2\theta}\right). \tag{4.9}$$

We emphasize that (4.9) makes it possible to determine the temporal variation of the shoreline motion for the complete runup/rundown event. Note that Synolakis (1987) and Tadepalli & Synolakis (1994) were limited by the convergence radius of (4.7) and consequently they could predict maximum runup but not rundown of solitary waves, maximum rundown but not runup of leading depression isosceles waves, and breaking during runup but not during rundown.

4.2. *The shoreline motion*

In order to determine the analytical expressions for the shoreline elevation and velocity, we combine (4.6), (4.8) and (4.9) with (4.4) and (4.4), which yields

$$\frac{\gamma V(\lambda)}{\Omega A_0\sqrt{\Omega t_0}} = 16\sqrt{2\pi}Li\left(-\frac{5}{2}, -\mathrm{e}^{2\theta}\right), \tag{4.10}$$

$$\frac{R(\lambda)}{A_0\sqrt{\Omega t_0}} = -8\sqrt{2\pi}Li\left(-\frac{3}{2}, -\mathrm{e}^{2\theta}\right) - \frac{V(\lambda)^2}{2gA_0\sqrt{\Omega t_0}}. \tag{4.11}$$

The variation of the three polylogarithms with respect to θ is shown in figure 3. The velocity polylogarithm Li (with $m=-5/2$) has a local minimum of -0.06273

https://doi.org/10.1017/S0022112009992485 Published online by Cambridge University Press

for $\theta = -0.9136$, and a maximum of 0.1156 for $\theta = 0.2786$, while the elevation polylogarithm (with $m = -3/2$) has a local maximum of 0.1517 for $\theta = -0.3657$, and a minimum of -0.06027 for $\theta = 1.2968$. Furthermore, the velocity polylogarithm (with $m = -5/2$) is zero when the elevation polylogarithm (with $m = -3/2$) has its maxima/minima. This also follows directly from the functional property (Wood 1992)

$$\frac{\partial Li(m, e^{\theta})}{\partial \theta} = Li(m-1, \mathrm{e}^{\theta}). \tag{4.12}$$

This makes it easy to determine the maximum runup and drawdown elevations and velocities from (4.11) and (4.11):

$$\frac{R_{up}}{A_0\sqrt{\Omega t_0}} = 3.043, \qquad \frac{R_{down}}{A_0\sqrt{\Omega t_0}} = -1.209, \tag{4.13}$$

$$\frac{\gamma V_{up}}{\Omega A_0\sqrt{\Omega t_0}} = -2.516, \qquad \frac{\gamma V_{down}}{\Omega A_0\sqrt{\Omega t_0}} = 4.636. \tag{4.14}$$

Obviously, the runup elevation is significantly larger than the rundown elevation, while the rundown velocity is significantly larger than the runup velocity. This is in contrast to the sinusoidal wave results (3.3)–(3.4), which are symmetric. We can also conclude that the runup elevation of a single hump will be smaller than that of a sinusoidal wave with the same crest level, while the maximum rundown velocity will be significantly greater.

4.3. *Breaking criterion for single waves*

We differentiate (4.11) with respect to λ by using the polylogarithmic property (4.12) and find that according to (2.23), the Jacobian will vanish if

$$\left(\frac{\Omega^2 A_0}{g\gamma^2}\sqrt{\Omega t_0}\right) 32\sqrt{2\pi} Li\left(-\frac{7}{2}, -\mathrm{e}^{2\theta}\right) = -1. \tag{4.15}$$

The variation of the acceleration polylogarithm Li (with $m = -7/2$) is shown in figure 3: The first minimum occurs during *runup* and yields -0.028047 for $\theta = -1.3642$, while the second and considerably larger minimum occurs during *rundown* and yields -0.07988 for $\theta = 0.7188$. Notice that in contrast to the sinusoidal case, breaking will not occur at the point of maximum rundown, but slightly earlier during the rundown motion. This leads to two different breaking criteria

$$\frac{A_0}{h_0} = 0.4445\left(\frac{\Omega^2 h_0}{g\gamma^2}\right)^{-5/4} \qquad \text{(during runup)}, \tag{4.16}$$

$$\frac{A_0}{h_0} = 0.1561\left(\frac{\Omega^2 h_0}{g\gamma^2}\right)^{-5/4} \qquad \text{(during rundown)}. \tag{4.17}$$

The smaller the number, the stronger the criterion. Hence, the breaking criterion for runup is almost three times weaker than the breaking criterion for rundown.

4.4. *The special case of solitary waves satisfying the KdV equation*

It is straight forward to utilize the single wave solutions, to derive runup expressions for solitary waves satisfying the KdV equation. In this case Ω is not a free choice, but it is tied to the nonlinearity of the wave via the relations

$$\Omega = Kc, \quad K = \frac{1}{h_0}\sqrt{\frac{3A_0}{4h_0}}, \quad c = \sqrt{g(h_0 + A_0)}. \tag{4.18}$$

We shall now insert these restrictions in our single wave solution and verify the outcome against the solitary wave solution of Synolakis (1987). For this purpose, we

https://doi.org/10.1017/S0022112009992485 Published online by Cambridge University Press

approximate the celerity by $\sqrt{gh_0}$ and obtain

$$\Omega t_0 = \frac{\Omega x_0}{\sqrt{gh_0}} \simeq K x_0 = \sqrt{\frac{3}{4}}\sqrt{\frac{A_0}{h_0}}\frac{x_0}{h_0} = \sqrt{\frac{3}{4}}\sqrt{\frac{A_0}{h_0}}\gamma^{-1} \tag{4.19}$$

and

$$\frac{\Omega A_0}{\sqrt{gh_0}} \simeq K A_0 = \sqrt{\frac{3}{4}}\left(\frac{A_0}{h_0}\right)^{3/2}. \tag{4.20}$$

By inserting (4.19)–(4.20) in (4.13)–(4.14) we get

$$\frac{R_{up}}{h_0} = 2.832\gamma^{-1/2}\left(\frac{A_0}{h_0}\right)^{5/4}, \qquad \frac{R_{down}}{h_0} = -1.125\gamma^{-1/2}\left(\frac{A_0}{h_0}\right)^{5/4}, \tag{4.21}$$

$$\frac{V_{up}}{\sqrt{gh_0}} = -2.028\gamma^{-3/2}\left(\frac{A_0}{h_0}\right)^{7/4}, \qquad \frac{V_{down}}{\sqrt{gh_0}} = 3.736\gamma^{-3/2}\left(\frac{A_0}{h_0}\right)^{7/4}. \tag{4.22}$$

Note that R_{up} in (4.21) is in agreement with (3.7) in Synolakis (1987). Expressions for R_{down}, V_{up} and V_{down} were not provided by Synolakis (1987).

Also the breaking criteria (4.16)–(4.17) are easy to translate from single waves to solitary waves, and by inserting (4.20) we obtain

$$\frac{A_0}{h_0} < 0.8183\ \gamma^{10/9} \qquad \text{(during runup)}, \tag{4.23}$$

$$\frac{A_0}{h_0} < 0.5139\ \gamma^{10/9} \qquad \text{(during rundown)}. \tag{4.24}$$

Note that (4.23) is identical to the breaking criterion for runup given by Synolakis (1987) in his (6.3). The condition for the more critical rundown phase was not provided by Synolakis (1987).

5. Runup solution for N-waves

The runup of leading depression waves (i.e. waves with a small negative leading wave followed by a higher positive one) has been studied by, e.g. Pelinovsky & Mazova (1992), Tadepalli & Synolakis (1994, 1996), Carrier *et al.* (2003) and Kânoğlu (2004).

In the following we describe the incident N-waves by two counter-acting single waves given by

$$\eta_i(x_0, t) = A_1 \operatorname{sech}^2\Omega_1(t - t_1) - A_2 \operatorname{sech}^2\Omega_2(t - t_2), \tag{5.1}$$

where the frequencies can be chosen freely to represent the phenomena at hand. The Fourier transform of (5.1) readily yields

$$\widetilde{\Phi}_i(\omega) = \sqrt{\frac{\pi}{2}}\left(\frac{A_1}{\Omega_1^2}\frac{\omega e^{i\omega t_1}}{\sinh\frac{\pi\omega}{2\Omega_1}} - \frac{A_2}{\Omega_2^2}\frac{\omega e^{i\omega t_2}}{\sinh\frac{\pi\omega}{2\Omega_2}}\right), \tag{5.2}$$

and the resulting contour integral can be split up into two parts, which are both well known from the previous single-wave calculation. We choose to simplify the formulation further by assuming that $\Omega_1 = \Omega_2 = \Omega$, and fix the phase shift between the two waves to be $\Omega(t_1 - t_2) = \pi/2$. Furthermore, we introduce the amplitude ratio $\mu \equiv A_2/A_1$ which covers the interval $0 \leqslant \mu \leqslant 1$. Now the isosceles N-wave is represented by $\mu = 1$, the generalized N-wave is represented by $0 < \mu < 1$, and the single wave considered in the previous section is represented by $\mu = 0$.

https://doi.org/10.1017/S0022112009992485 Published online by Cambridge University Press

It should be emphasized that the crest elevation of the incoming N-waves depends on μ: For $\mu = 0$ it is A_1, and then it drops gradually to $0.8585A_1$ for the case of $\mu = 1$. Obviously, this difference should be taken into consideration if the runup of two different N-waves is to be compared in absolute terms. On the other hand, it may be more relevant for a fair comparison to require similarity in incoming potential/kinetic energy rather than in wave crest elevation. We shall not pursue this issue any further in this work.

The resulting shoreline motion follows directly from (4.11)–(4.11), i.e.

$$\frac{\gamma V(\lambda)}{\Omega A_1\sqrt{\Omega t_0}} = 16\sqrt{2\pi}\Gamma_\mu\left(\frac{5}{2},\theta,\mu\right), \tag{5.3}$$

$$\frac{R(\lambda)}{A_1\sqrt{\Omega t_0}} = -8\sqrt{2\pi}\Gamma_\mu\left(\frac{3}{2},\theta,\mu\right) - \frac{V(\lambda)^2}{2gA_1\sqrt{\Omega t_0}}, \tag{5.4}$$

where

$$\Gamma_\mu(m,\theta,\mu) \equiv Li(-m,-\mathrm{e}^{2\theta}) - \mu Li(-m,-\mathrm{e}^{2\theta+\pi}), \quad \theta \equiv \Omega(\lambda - t_1 - 2t_0). \tag{5.5}$$

The variation of $\Gamma_\mu(m,\theta,\mu)$ with respect to θ is shown in figure 4(a) for $m = 3/2$ (elevation) and in figure 4(b) for $m = 5/2$ (velocity) for $\mu = 0$, 0.25, 0.5 and 1. We notice that the first maximum draw-down occurs at $\theta \simeq -2$ (for $\mu > 0$), followed by the first maximum runup occurring at $\theta \simeq -0.35$, and then the second maximum draw-down at $\theta \simeq 1.35$. We also notice that in agreement with (4.12), the elevation peaks whenever the velocity is zero.

The maxima/minima of the shoreline velocities and elevations can be expressed as

$$\frac{\gamma V_{up/down}}{\Omega A_1\sqrt{\Omega t_0}} = \chi_{velo}(\mu), \qquad \frac{R_{up/down}}{A_1\sqrt{\Omega t_0}} = \chi_{elev}(\mu), \tag{5.6}$$

and figure 5 shows the variation of χ_{velo} and χ_{elev} as a function of μ for the first draw-down (1), the following runup (2) and the second draw-down (3). Generally, the runup elevation is always larger than any of the draw-down elevations, and it increases with μ, i.e. the runup increases when the negative forerunner in the leading depression becomes larger. For $\mu < 0.62$ the draw-down velocity exceeds the runup velocity, and vice versa for $\mu > 0.62$. For the special case of $\mu = 1$ (the isosceles N-wave) we get

$$\chi_{velo}(1) = \begin{cases} 2.259 & (\theta = -2.527), \\ -6.687 & (\theta = -1.214), \\ 5.204 & (\theta = 0.281), \end{cases} \qquad \chi_{elev}(1) = \begin{cases} -2.676 & (\theta = -2.010), \\ 4.243 & (\theta = -0.345), \\ -0.712 & (\theta = 1.438). \end{cases}$$

Notice that although the incoming isosceles is a symmetric wave, the runup and draw-down solutions are not symmetric. We also notice that the elevation and velocity coefficents are generally different. Both observations are in contrast to the sinusoidal wave solution (3.3)–(3.4), which yields $\chi_{elev} = \chi_{velo} = \pm 2\sqrt{\pi} \simeq \pm 3.5449$.

5.1. *Breaking criterion for N-waves*

We differentiate (5.4) with respect to λ by using the polylogarithmic property (4.12) and find that according to (2.23), the Jacobian will vanish if

$$\left(\frac{\Omega^2 A_1}{g\gamma^2}\sqrt{\Omega t_0}\right) 32\sqrt{2\pi}\Gamma_\mu\left(\frac{7}{2},\theta,\mu\right) = -1. \tag{5.7}$$

Figure 4(c) shows the variation of $\Gamma_\mu(7/2,\theta,\mu)$ with respect to θ for $\mu = 0$, 0.25, 0.5 and 1. We notice that the minima generally occur just after the first maximum

https://doi.org/10.1017/S0022112009992485 Published online by Cambridge University Press

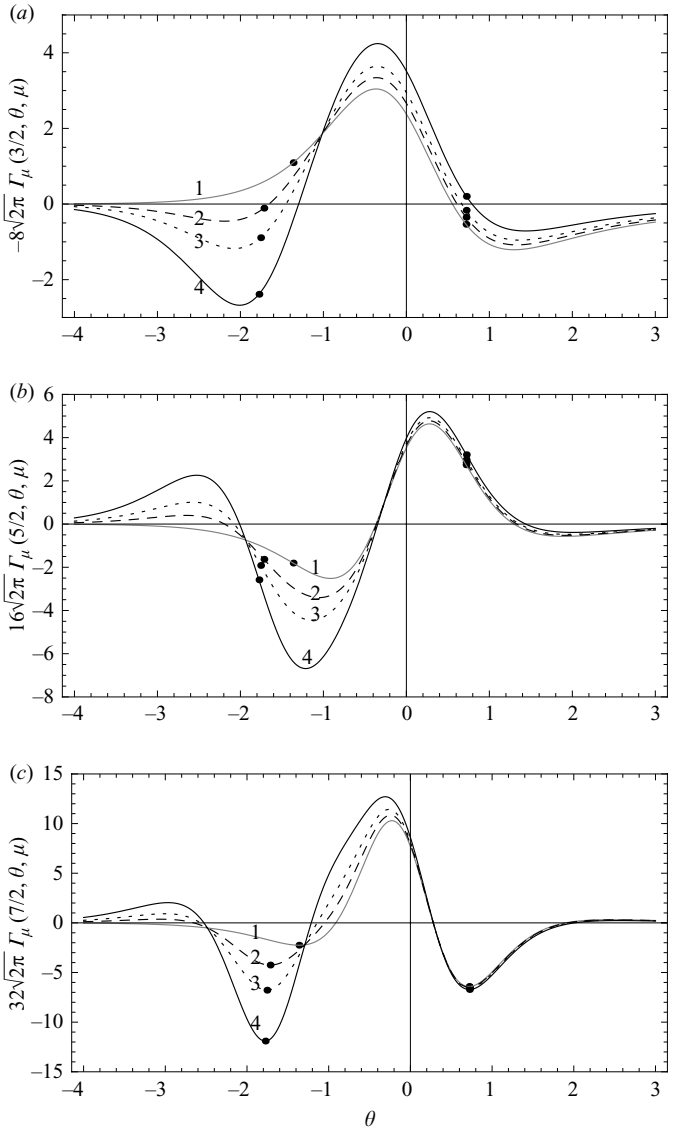


FIGURE 4. Temporal variation of the relevant polylogarithms for shoreline motions of leading depression N-waves. (a) Elevation polylogarithm ($m=-3/2$); (b) velocity polylogarithm ($m=-5/2$); (c) acceleration polylogarithm ($m=-7/2$). 1: $\mu=0$; 2: $\mu=0.25$; 3: $\mu=0.50$; 4: $\mu=1.0$. Location of possible breaking shown as markers on each curve.

rundown (i.e. during runup) and just before the second maximum rundown (i.e. during rundown). The locations of these events are shown in figure 4(a–c) as markers on the elevation, velocity and acceleration polylogarithms. The corresponding breaking criteria can be expressed as

$$\frac{A_1}{h_0} = \chi_{break}(\mu)\left(\frac{\Omega^2 h_0}{g\gamma^2}\right)^{-5/4}, \tag{5.8}$$

where the variation of χ_{break} with μ is shown in figure 6. The smaller the number the stronger the criterion. We notice that the strongest criterion occurs during rundown

https://doi.org/10.1017/S0022112009992485 Published online by Cambridge University Press

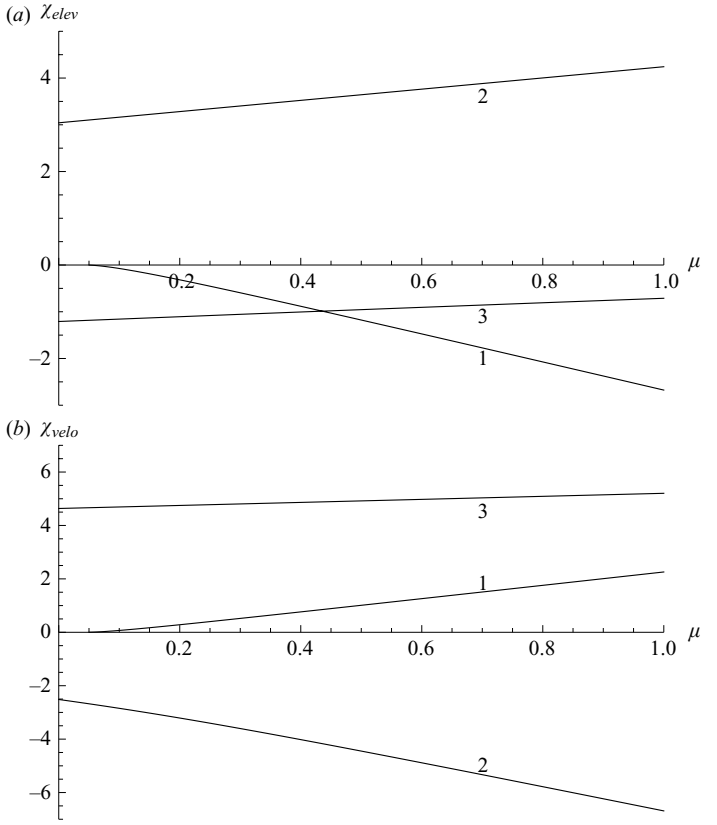


FIGURE 5. Maximum runup/rundown elevations and velocities for leading depression N-waves as a function of $\mu = A_2/A_1$. (*a*) Shoreline elevation; (*b*) shoreline velocity. (1) first rundown; (2) runup; (3) second rundown.

for $\mu < 0.48$, and during runup for $\mu > 0.48$. In all cases the criteria are stronger than for sinusoidal waves, which yields $\chi_{break} = (2\sqrt{\pi})^{-1} \simeq 0.282$.

6. Comparison of sinusoidal waves, single waves and N-waves

We emphasize that the different maxima and minima of the shoreline velocities and elevations for sinusoidal waves, single waves and N-waves presented in §§ 3, 4 and 5, can all be expressed on the form

$$\frac{R_{up/down}}{A_0\sqrt{\Omega t_0}} = \chi_{elev}, \qquad \frac{\gamma V_{up/down}}{\Omega A_0\sqrt{\Omega t_0}} = \chi_{velo}, \tag{6.1}$$

where γ is the bed slope, Ω is the wave frequency which defines the wave duration and A_0 is the wave amplitude of the incoming wave at $x = x_0$ $(= h_0/\gamma)$. Note that on the basis of the formulations by Synolakis (1987) and Tadepalli & Synolakis (1994), Geist (1999) came to the conclusion that 'for N-waves the relationship between the amplitude of the incident wave and the maximum runup is not a linear one and that R is proportional to the amplitude to the power 5/4'. We can now conclude that the relationship is indeed a linear one for all possible wave forms, and that the apparent nonlinearity in the expressions by Synolakis (1987) and Tadepalli & Synolakis (1994) is caused by their specific solitary wave tie between frequency and wave amplitude.

https://doi.org/10.1017/S0022112009992485 Published online by Cambridge University Press

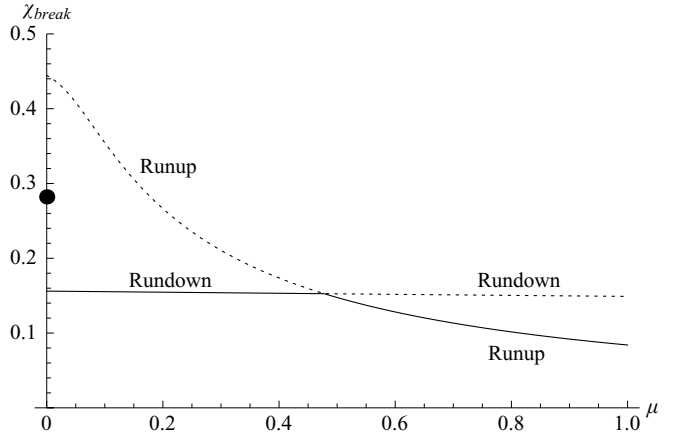


FIGURE 6. Breaking criteria for leading depression N-waves as a function of $\mu = A_2/A_1$. Full line indicates the strongest breaking criteria. The marker indicates the breaking criterion for sinusoidal waves.

Our result is in agreement with earlier findings by Pelinovsky & Mazova (1992) and Didenkulova *et al.* (2007).

Alternatively, we can reformulate (6.1) by using that $t_0 = x_0/\sqrt{gh_0} = \sqrt{h_0/(g\gamma^2)}$, which yields

$$\frac{R_{up/down}}{A_0} = \chi_{elev}\left(\frac{\Omega^2 h_0}{g\gamma^2}\right)^{1/4}, \qquad \frac{\gamma V_{up/down}}{\Omega A_0} = \chi_{velo}\left(\frac{\Omega^2 h_0}{g\gamma^2}\right)^{1/4}, \tag{6.2}$$

and similarly the different theoretical breaking criteria established in §§ 4, 5 and 6 can all be expressed on the form

$$\frac{A_0^{break}}{h_0} = \chi_{break}\left(\frac{\Omega^2 h_0}{g\gamma^2}\right)^{-5/4}. \tag{6.3}$$

Note that the maximum values of $R_{up/down}$ and $V_{up/down}$ occur whenever $A_0 = A_0^{break}$, and by inserting (6.3) in (6.2) we obtain the limiting results

$$\frac{R_{up/down}^{limit}}{h_0} = \chi_{elev}\chi_{break}\left(\frac{\Omega^2 h_0}{g\gamma^2}\right)^{-1}, \qquad \frac{\gamma V_{up/down}^{limit}}{\Omega h_0} = \chi_{velo}\chi_{break}\left(\frac{\Omega^2 h_0}{g\gamma^2}\right)^{-1}. \tag{6.4}$$

As shown by Madsen & Fuhrman (2008), it is convenient to introduce the classical surf-similarity parameter, which was established by Battjes (1974) for the description of breaking wind waves in the surf zone. This parameter is defined by $\xi \equiv \gamma/\sqrt{H_0/L_\infty}$, where $L_\infty = gT^2/(2\pi)$. If we interpret T as the duration (i.e. $2\pi/\Omega$) rather than the wave period, we obtain

$$\xi = \sqrt{\pi}\left(\frac{A_0}{h_0}\right)^{-1/2}\left(\frac{\Omega^2 h_0}{g\gamma^2}\right)^{-1/2}, \tag{6.5}$$

by which (6.2) and (6.4) can be expressed by

$$\frac{R_{up/down}}{A_0} = \chi_{elev}\pi^{1/4}\left(\frac{A_0}{h_0}\right)^{-1/4}\xi^{-1/2}, \qquad \frac{R_{up/down}^{limit}}{A_0} = \frac{\chi_{elev}\chi_{\mathrm{break}}}{\pi}\xi^2, \tag{6.6}$$

https://doi.org/10.1017/S0022112009992485 Published online by Cambridge University Press

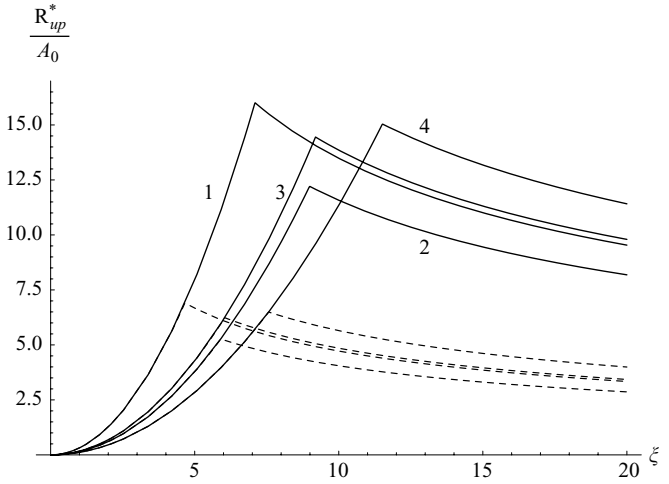


FIGURE 7. Maximum relative run-up as a function of the surf similarity parameter (ξ). Full lines: $A_0/h_0 = 0.00015$; dashed lines: $A_0/h_0 = 0.01$. (1) Sinusoidal wave ($\chi_{elev} = 2\sqrt{\pi}$, $\chi_{break} = (2\sqrt{\pi})^{-1}$). (2) Single wave ($\chi_{elev} = 3.043$, $\chi_{break} = 0.1561$). (3) N-wave with $\mu = 0.5$ ($\chi_{elev} = 3.642$, $\chi_{break} = 0.1475$). (4) Isosceles wave with $\mu = 1$ ($\chi_{elev} = 4.243$, $\chi_{break} = 0.084$).

$$\frac{V_{up/down}}{\sqrt{gA_0}} = \chi_{velo}\pi^{3/4}\left(\frac{A_0}{h_0}\right)^{-1/4}\xi^{-3/2}, \qquad \frac{V^{limit}_{up/down}}{\sqrt{gA_0}} = \frac{\chi_{velo}\chi_{break}}{\sqrt{\pi}}\xi. \tag{6.7}$$

Figure 7 shows the variation of R^*_{up}/A_0, where $R^*_{up} \equiv \min(R_{up}, R^{limit}_{up})$ and where χ_{break} is the smallest relevant value for the particular wave shape. The solutions are shown as a function of ξ for two different values of A_0/h_0 and for four different wave shapes: (1) sinusoidal waves; (2) single waves; (3) N-wave with $\mu = 0.5$; (4) isosceles wave with $\mu = 1$. The full lines represent $A_0/h_0 = 0.00015$, while the dashed lines represent $A_0/h_0 = 0.01$. We notice that for a certain value of ξ, which allows for non-breaking waves of all four types, it is clear that the isosceles wave leads to the highest runup, while the single wave leads to the lowest. For a given wave shape and a given value of A_0/h_0, the relative runup R_{up}/A_0 increases for decreasing values of ξ as long as breaking does not occur. The smaller the A_0/h_0, the larger the amplification R_{up}/A_0. The theoretical limit of the runup solutions is defined by R^{limit}_{up}/A_0, and it is a function of ξ but not a function of A_0/h_0. This curve will intersect and limit the runup curves at $\xi = \xi^{break}$, and the smaller the A_0/h_0, the larger the ξ^{break}. It is also clear that ξ^{break} is generally higher for N-waves than for sinusoidal waves i.e. they break much more easily and on steeper slopes. For a given long wave, the worst case scenario is a beach which corresponds to $\xi = \xi^{break}$. Beyond this point, i.e. for $\xi < \xi^{break}$, the theoretical solutions are not valid. One may speculate if the runup of breaking waves will follow the limiting curve R^{limit}_{up} corresponding to some sort of saturated breaker model. This assumption is, however, not correct as documented by laboratory measurements of, e.g. breaking sinusoidal waves and breaking solitary waves, which result in runups much larger than predicted by R^{limit}_{up} (see e.g. Synolakis 1987; Madsen & Fuhrman 2008). The runup of breaking wave events is beyond the scope of the present work.

Figure 8(a–c) shows the shoreline motion due to incoming sinusoidal waves, single waves and N-waves for a specific test case. We consider an offshore depth $h_0 = 4000$ m, and a beach slope $\gamma = 1/75$ i.e. $x_0 = 300$ km, $t_0 = 1514$ s and $c = \sqrt{gh_0} = 198$ m s^{-1}.

https://doi.org/10.1017/S0022112009992485 Published online by Cambridge University Press

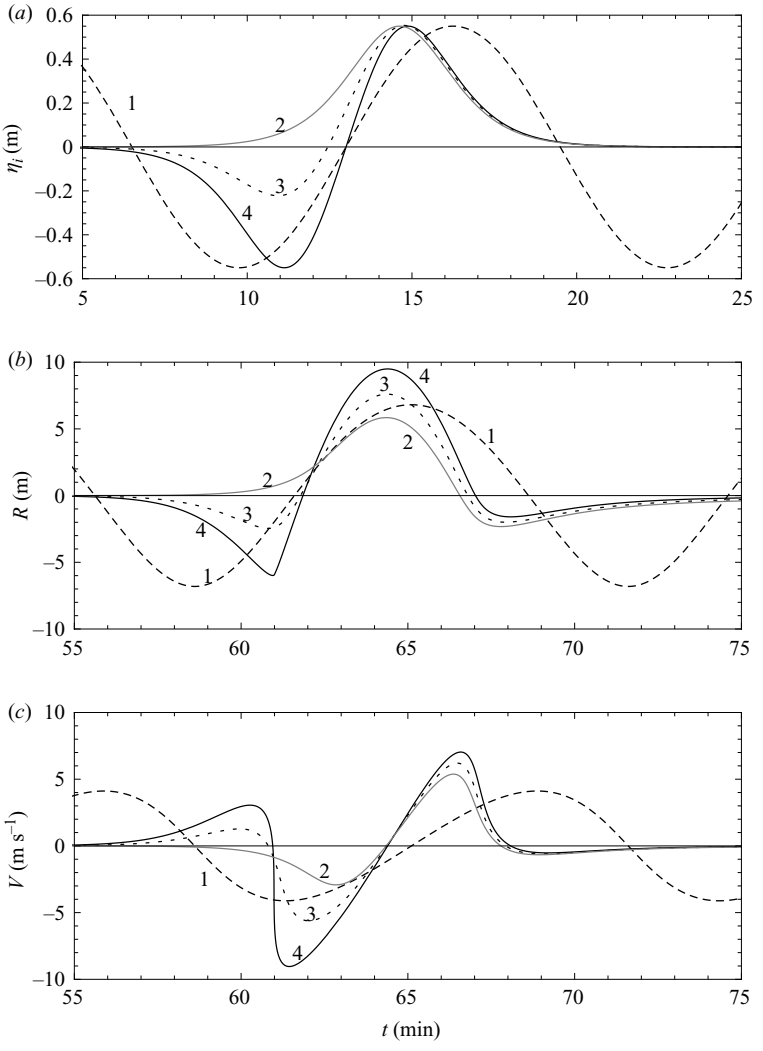


FIGURE 8. Shoreline motion due to incoming sinusoidal waves, single waves and N-waves. Specifications: $h_0 = 4000$ m, $\gamma = 1/75$, $T = 13$ min, $\Omega = 2\pi/T$. (1) Sinusoidal wave ($A_0 = 0.55$ m). (ii) Single wave ($A_0 = 0.55$ m). (3) Leading depression wave ($A_1 = 0.60$ m, $\mu = 0.5$). (4) Isosceles depression wave ($A_1 = 0.64$ m, $\mu = 1.0$). (a) Incoming surface elevation at $x = x_0$; (b) shoreline elevation; (c) shoreline velocity.

The wave period is chosen to be $T = 13$ min as a typical tsunami period, and with $\Omega = 2\pi/T$ we get $2t_0\Omega \simeq 24$, i.e. significantly larger than 4.88 as required in connection with (2.36). The incoming time series are described by $\eta_1(x_0, t) = A_0 \cos(\Omega(t - t_1) - \pi/2)$ for the sinusoidal wave, by $\eta_2(x_0, t) = A_0 \operatorname{sech}^2(\Omega(t - t_1) - \pi/4)$ for the single wave and by $\eta_3(x_0, t) = A_1 \left(\operatorname{sech}^2(\Omega(t - t_1) - \pi/4) - \mu \operatorname{sech}^2(\Omega(t - t_1) + \pi/4)\right)$ for the N-waves. In all cases we use $t_1 = T$. The incoming wave amplitudes for the different wave theories are chosen so that the crest level is the same at $x = x_0$. This leads to (1) $A_0 = 0.55$ m (sinusoidal wave); (2) $A_0 = 0.55$ m (single wave); (3) $A_1 = 0.60$ m (N-wave with $\mu = 0.5$); d) $A_1 = 0.64$ m (isosceles N-wave with $\mu = 1$). The incoming time series are shown in figure 8(a). The runup is determined by using the analytical expressions (3.4)–(3.3) for the sinusoidal waves, and (5.4)–(5.4) for the N-waves. The

https://doi.org/10.1017/S0022112009992485 Published online by Cambridge University Press

resulting temporal variations of the shoreline elevation and velocity are depicted in figure 8(*b–c*). It should be emphasized that we get exactly the same solution by invoking the convolution integrals given by (2.42)–(2.43). All four cases correspond to $A_0/h_0 \simeq 0.00015$ and $\xi \simeq 12$. According to figure 7, this is on the edge of wave breaking for the isosceles wave, while the other wave forms are further from breaking. Consequently, figure 8(*a–c*) shows that the isosceles wave leads to the highest runup, while the single wave leads to the smallest. This is in good agreement with figure 7. All the N-wave profiles are significantly steeper than the sinusoidal wave, and thus their runup/rundown velocities are significantly higher, again with the isosceles wave leading to the largest velocities.

Finally, let us consider the possibility of using solitary wave theory to represent the single wave in figure 8(*a–c*). In this case the incoming time series will be described by $\eta_4(x_0, t) = A_4 \operatorname{sech}^2(\Omega_s(t - t_1) - \pi/4)$ where

$$\Omega_s = c_s K_s, \qquad K_s = \frac{1}{h_0}\sqrt{\frac{3}{4}\frac{A_4}{h_0}}, \qquad c_s = \sqrt{g(h_0 + A_4)}.$$

If we choose to match the incoming wave heights, i.e. $A_4 = A_0 = 0.55$ m, the resulting effective wave period $T_s = 2\pi/\Omega_s$ becomes 16 times larger than $T = 13$ min. In this case the maximum runup elevation on the beach becomes 1.46 m for the solitary wave in contrast to the 5.84 m reached by the single wave in figure 8(*b*). Alternative if we choose to match the wave periods, i.e. $T_s = T = 13$ min, this requires that $A_4 = 136$ m on the depth of $h_0 = 4000$ m. This example demonstrates the problem of using solitary wave theory to represent tsunamis. If applied in deep water, the solitary theory will typically result in effective periods which are much too large. On the other hand, if applied in shallow water (which is the case for most experimental investigations), the solitary theory will result in periods which are much too small: As an example a wave height of 6 m in a depth of 30 m leads to $T_s = 26$ s. It is obviously necessary to be able to choose the temporal and spatial scales independently of the wave height to water depth ratio and for this reason we do not recommend to apply solitary wave theory for tsunamis.

7. Runup solution for transient waves

A time series of an incident tsunami hitting the beach would typically originate from a distant disturbance caused by a seismic event in the deep ocean. This disturbance would generate a transient wave of extremely small nonlinearity and very small dispersion, and any abrupt features of the initial disturbance would gradually be smoothed over long-travel distances by the effect of dispersion. In this section we consider the canonical situation where the nonlinear runup on the slope is preceded by long-distance transformation of linear transient waves over a constant depth. This part of the problem is adequately modelled by the linear KdV equation, which captures the weak dispersion of the leading waves in the wavetrain.

7.1. *Exact solutions to the linear KdV equation on a constant depth*

According to Whitham (1974), his § 13.6, an exact solution to the linear KdV equation reads

$$\eta_\delta(\chi, \tau) = \left(\frac{2}{\tau}\right)^{1/3} Ai(Z(\chi, \tau)), \tag{7.1}$$

https://doi.org/10.1017/S0022112009992485 Published online by Cambridge University Press

where Ai is the Airy function, and where

$$\chi \equiv \frac{\widehat{x}}{h_0}, \qquad \tau \equiv t\sqrt{\frac{g}{h_0}}, \qquad Z(\chi,\tau) \equiv (\chi-\tau)\left(\frac{2}{\tau}\right)^{1/3}. \tag{7.2}$$

Here $\widehat{x}$ is a shoreward directed horizontal coordinate being zero at the front of the initial disturbance, while the travel distance over constant depth is denoted $\widehat{x}_0$ and the distance up the slope is $x_0 = h_0/\gamma$. Hence in terms of the runup coordinate system defined in figure 1, we have that $(\widehat{x}-\widehat{x}_0) = -(x-x_0)$. Whitham (1974) points out that (7.1) is actually the impulse response function to the problem, where the initial condition is described as a delta function at $\widehat{x}=0$. We are interested in the general initial condition

$$\eta_0(\chi,0) = \begin{cases} F(\chi) & \text{for} \quad \chi_1 < \chi < 0, \\ 0 & \text{otherwise}, \end{cases} \tag{7.3}$$

in which case (7.1) should be generalized to the convolution integral

$$\eta(\chi,\tau) = \int_{-\infty}^{\infty} F(\chi-y)\eta_\delta(y,\tau)\,\mathrm{d}y, \tag{7.4}$$

and from the bounds of (7.3) we find that $\chi_1 < \chi - y < 0 \quad \Rightarrow \quad \chi < y < \chi - \chi_1$. Hence (7.4) can be simplified to

$$\eta(\chi,\tau) = \left(\frac{2}{\tau}\right)^{1/3} \int_{\chi}^{\chi-\chi_1} F(\chi-y)Ai(Z(y,\tau))\,\mathrm{d}y, \tag{7.5}$$

and by changing the integration variable from $y=\chi$ to $s=Z(\chi,\tau)$ this becomes

$$\eta(\chi,\tau) = \int_{Z(\chi,\tau)}^{Z(\chi-\chi_1,\tau)} F\left((Z(\chi,\tau)-s)\left(\frac{2}{\tau}\right)^{-1/3}\right) Ai(s)\,\mathrm{d}s. \tag{7.6}$$

Note that if $F(x)$ simplifies to a Heaviside Unitstep function with amplitude a, we get $\chi_1 \to -\infty$, and (7.6) simplifies to

$$\eta(\chi,\tau) = \int_{Z(\chi,\tau)}^{\infty} aAi(s)\,\mathrm{d}s, \tag{7.7}$$

which is the expression discussed by Whitham (1974), § 13.6.

We consider a dipole source made up of two rectangular disturbances covering the intervals $\chi_1 < \chi < 0$ with the amplitude a_1 and $\chi_2 < \chi < \chi_1$ with the amplitude a_2. In this case (7.6) simplifies to

$$\eta(\chi,\tau) = \int_{Z(\chi,\tau)}^{Z(\chi-\chi_1,\tau)} a_1 Ai(s)\,\mathrm{d}s + \int_{Z(\chi-\chi_1,\tau)}^{Z(\chi-\chi_2,\tau)} a_2 Ai(s)\,\mathrm{d}s. \tag{7.8}$$

We note that the difference between the lower and upper bounds of the integral in (7.8) effectively shrinks over time according to (7.2). By the use of (7.8) we can now easily determine the evolution of the initial disturbance while it travels on a constant depth in the deep ocean. Madsen *et al.* (2008) showed that (7.8) was in excellent agreement with numerical simulations based on a high-order Boussinesq model for linear waves travelling up to 5000 water depths.

7.2. *The runup of transient waves caused by a monopole source*

By combining the convolution integrals (2.42)–(2.43) with (7.8) we can now easily capture the prevailing features of the entire process starting with an initial disturbance

https://doi.org/10.1017/S0022112009992485 Published online by Cambridge University Press

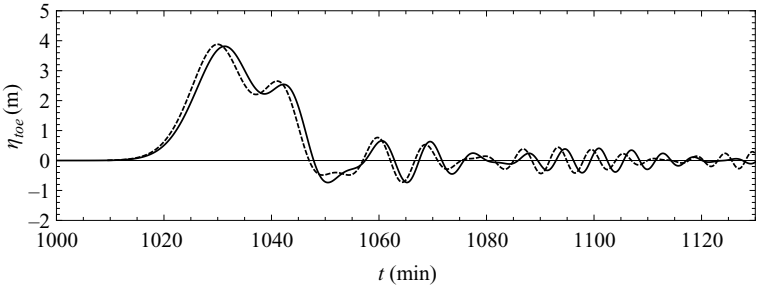


FIGURE 9. Surface elevation at the toe of the slope due to a monopole source. Full line: analytical theory based on (7.8); dashed line: numerical model ($dx = 400$ m, $dt = 2.0$ s). Specifications: $h_0 = 4000$ m, $a_1 = 0$, $a_2 = 3.0$ m, $\hat{x}_1 = -150$ km, $\hat{x}_2 = -400$ km, $\hat{x}_0 = 12\,000$ km.

of arbitrary shape in the deep ocean, followed by long-distance evolution under the influence of weak dispersion, and eventually leading to nonlinear shoaling and runup on a plane sloping beach. We shall verify the outcome of this very swift and semi-analytical calculation with numerical results obtained from a numerical model, which solves the high-order Boussinesq formulation by Madsen, Fuhrman & Wang (2006). The numerical solution procedure is based on finite difference discretizations on an equidistant grid, and an explicit four-stage fourth-order Runge–Kutta scheme is used for the time integration. A detailed description of the scheme can be found in Madsen, Bingham & Liu (2002) for one horizontal dimension, and in Fuhrman & Bingham (2004) for two horizontal dimensions. The special runup feature in the model uses a simple linear extrapolation of variables at wet-dry boundaries and has been described and validated recently in Fuhrman & Madsen (2008).

First, we investigate the case of a monopole source described by a single rectangular disturbance with amplitude 3.0 m covering the interval from $\widehat{x}_1 = -150$ km to $\widehat{x}_2 = -400$ km. The offshore depth is $h_0 = 4000$ m, and the toe of the slope is located at $\widehat{x}_0 = 3000\,h_0 = 12\,000$ km. The beach slope is $\gamma = 1/75$, i.e. the width of the slope is $x_0 = h_0/\gamma = 300$ km. As a result, the incoming transient waves showing up at the toe of the slope can be estimated by the dipole formulation (7.8) using $a_1 = 0$ m, $a_2 = 3.0$ m, $\chi_1 = \widehat{x}_1/h_0 = -37.5$, $\chi_2 = \widehat{x}_2/h_0 = -100$ and $\chi = \widehat{x}_0/h_0 = 3000$. This is shown as a full line in figure 9. The corresponding numerical solution obtained by the Boussinesq model will generally contain the additional effect of wave reflection from the slope, hence to make sure that the computed time series at the toe contains only the incoming wave, we have (in a separate run) simulated the wave propagation without the sloping entrance to the beach. A fixed grid size of 400 m is used leading to a total of 33 000 grid points, while the time step is 2 s leading to a total of 36 000 time steps. The result of this computation is shown in figure 9 as the dotted line. In general, we notice that the bulk of the disturbance covers about 40 min and contains two peaks separated by approximately 12 min. Behind the hump, the tail contains wave groups with shorter and shorter waves and eventually the weakly dispersive analytical approach will become inadequate. However, the shortest waves within the time window shown in figure 9 have periods of approximately 6 min corresponding to $kh_0 \simeq 0.36$ for which the linear KdV theory still provides sufficient accuracy. Nevertheless, we do observe phase differences between the analytical (full line) and computed (dashed line) solutions in figure 9: The computed wave arrives approximately 1 min earlier and it is slightly steeper. This is mainly due to amplitude dispersion: The front of the wave has an amplitude of $b = 4$ m and it will propagate

https://doi.org/10.1017/S0022112009992485 Published online by Cambridge University Press

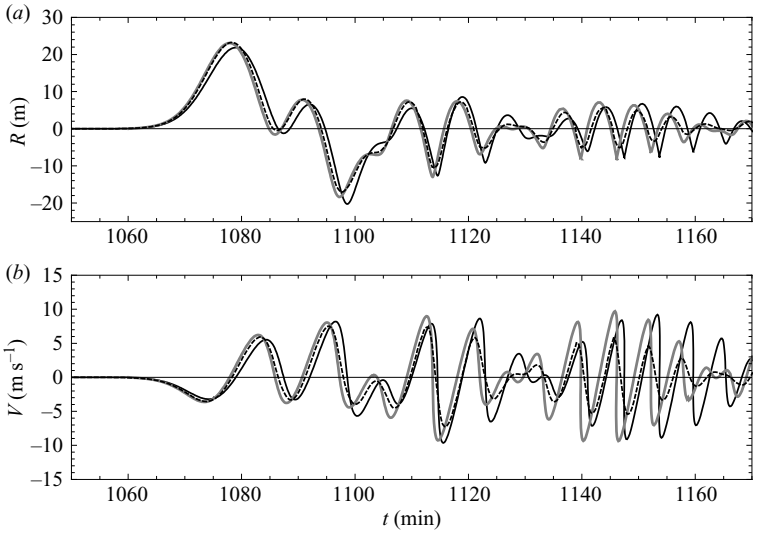


FIGURE 10. Shoreline motion due to a monopole source. Full line (black): analytical theory from source to beach, i.e. based on the analytical solution from figure 9; full line (grey): analytical theory from toe to beach, i.e. based on the numerical solution from figure 9; dashed line: numerical model from source to beach ($\mathrm{d}x = 400$ m, $\mathrm{d}t = 2.0$ s). (*a*) Shoreline elevation; (*b*) shoreline velocity. Specifications: $h_0 = 4000$ m, $a_1 = 0$, $a_2 = 3.0$ m, $\hat{x}_1 = -150$ km, $\hat{x}_2 = -400$ km, $\hat{x}_0 = 12\,000$ km, $x_0 = 300$ km, $\gamma = 1/75$.

with the celerity $c_n = \sqrt{g(h_0 + b)} \simeq 198.19$ m s^{-1}, while the front of the analytical solution effectively propagates with $c_0 = \sqrt{gh_0} \simeq 198.09$ m s^{-1}. Although this effect is extremely small, it accumulates to an arrival time deficit of approximately -30 s over the distance of 12 150 km. Overall, however, we see a good agreement between the analytical and computed time series at the toe of the slope, which confirms that (7.8) provides a very effective estimate of the processes in the deep ocean.

Once the waves reach the toe of the slope and start the shoaling process towards the shore, frequency dispersion is completely neglected in the analytical method. Hence, in reality, the shorter waves will be slightly delayed during their runup compared to the theory, but this effect can be shown to be quite insignificant for the present wavetrain due to the relatively short travel distance. We determine the analytical shoreline motion by using the convolution integrals (2.42)–(2.43) combined with the time series of the incoming surface elevation at the toe. Figure 10 shows two analytical calculations: (1) A *source-to-beach* calculation based on the analytical solution at the toe (shown as the full black line); (2) A *toe-to-beach* calculation based on the computed time series at the toe (shown as the full grey line). The runup elevation and shoreline velocity are shown in figures 10(*a*) and 10(*b*), respectively. The initial runup elevation becomes approximately 22 m and after the main hump has passed a similar rundown occurs. Then a tail of wave groups with shorter waves shows up. The two analytical results are quite similar except for a phase shift.

Figure 10(*a*, *b*) also show the numerical shoreline computations using the fixed grid of 400 m all the way from the source to the shoreline. Although this grid size is somewhat coarse for the runup region, it is adequate for the leading long waves in the transient wavetrain resulting in a relatively large runup excursion (order 4 km) and a large distance from maximum draw-down to the first offshore crest in the standing wavetrain (order 6 km). From figure 10(*a*, *b*) we notice a fairly good agreement

https://doi.org/10.1017/S0022112009992485 Published online by Cambridge University Press

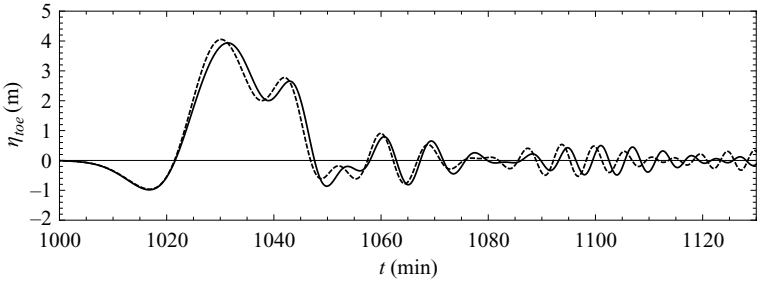


FIGURE 11. Surface elevation at the toe of the slope due to a dipole source. Full line: analytical theory based on (7.8); dashed line: numerical model ($dx = 400$ m, $dt = 2.0$ s). Specifications: $h_0 = 4000$ m, $a_1 = -1.0$ m, $a_2 = 3.0$ m, $\hat{x}_1 = -150$ km, $\hat{x}_2 = -400$ km, $\hat{x}_0 = 12\,000$ km.

between the numerical solution and the two analytical calculations up to $t \simeq 1120$ min. The *toe-to-beach* calculation is in better agreement with the numerical runup than the *source-to-beach* calculation, but the main features of the runup are captured by both solutions. Beyond the time of 1120 min, discrepancies between the analytical and numerical solutions start to show up and they are most pronounced in the shoreline velocity. The reason is that the chosen grid size of 400 m is too coarse to provide an accurate runup of the shorter waves, because they have shoreline excursions of typically 800 m and a distance to the first offshore crest of only 1600 m. When the grid becomes too coarse the runup algorithm, which is based on linear extrapolation, will typically lead to a severe underestimation of the maximum drawdown and of the shoreline velocities, as seen in figure 10(*a*, *b*).

Finally, it should be emphasized that the runup transfer functions for elevation and especially for the velocity continuously increase with decreasing wave periods (see e.g. figure 2), and this trend will only be stopped by the process of wave breaking. We do not have a theoretical threshold for wave breaking of transient waves, but in fact breaking will clearly show up in the analytical results and it will manifest as very steep and double valued velocity time series, while the runup elevations will show a 'fishtail' variation near maximum rundown. This condition is almost reached in figure 10(*a*) after the hump has passed for $t > 1140$ min.

7.3. *The runup of transient waves caused by a dipole source*

Next, we investigate the case of a dipole source described by two adjacent rectangular disturbances with $a_1 = -1.0$ m covering the interval from $\hat{x} = 0$ to $\hat{x}_1 = -150$ km and by $a_2 = 3.0$ m covering the interval from $\hat{x}_1$ to $\hat{x}_2 = -400$ km. All other specifications are the same as before. The incoming transient waves at the toe of the slope are estimated by the dipole formulation (7.8) and the result is shown as a full line in figure 11. For comparison, the numerical solution excluding reflections from the slope is shown as the dashed line in figure 11. The quality of the agreement is similar to the case of the monopole source from figure 9.

Figure 12(*a*, *b*) show the resulting shoreline elevation and velocity. Again we determine two analytical solutions for the shoreline motion: a *source-to-beach* calculation based on the analytical solution at the toe (shown as full black line) and a *toe-to-beach* calculation based on the computed time series at the toe (shown as full grey line). The initial runup becomes approximately 28 m and after the main hump has passed a similar rundown occurs. Then a tail of wave groups shows up and they are similar to the tail for the monopole source shown in figure 10. For the

https://doi.org/10.1017/S0022112009992485 Published online by Cambridge University Press

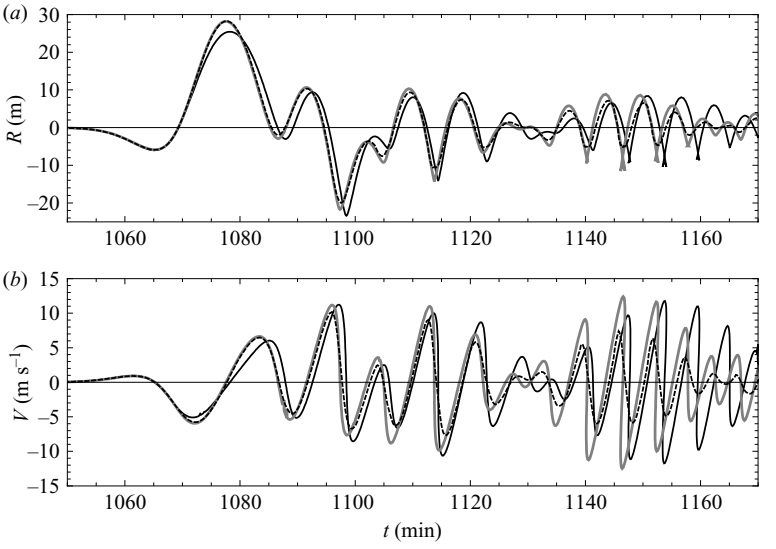


FIGURE 12. Shoreline motion due to a dipole source. Full line (black): analytical theory from source to beach, i.e. based on the analytical solution from figure 11; full line (grey): analytical theory from toe to beach, i.e. based on the numerical solution from figure 11; dashed line: numerical model from source to beach ($dx = 400$ m, $dt = 2.0$ s). (*a*) Shoreline elevation; (*b*) shoreline velocity. Specifications: $h_0 = 4000$ m, $a_1 = -1.0$ m, $a_2 = 3.0$ m, $\hat{x}_1 = -150$ km, $\hat{x}_2 = -400$ km, $\hat{x}_0 = 12\,000$ km, $x_0 = 300$ km, $\gamma = 1/75$.

main hump of the tsunami i.e. up to approximately 1120 min the agreement between the numerical and analytical solutions is quite good.

We note that the 'fishtail' variation in the runup elevation, which heralds the break down of NSW theory, is more pronounced for the dipole than for the monopole (figure 12 versus figure 10). It is also clear that although the two input signals reach the same maximum elevation at the foot of the slope (figures 9 and 11), the leading depression in the dipole amplifies the maximum runup elevation as well as the runup velocity compared to the monopole case. This conclusion supports equivalent observations in figure 8 in comparison between single waves and *N*-waves.

8. Summary and conclusion

In this work we have considered the runup of nonlinear long waves propagating from an offshore constant depth region to a plane sloping beach. The waves are assumed to obey the linear shallow-water equations or the linear KdV equation in the constant depth offshore region, while they are assumed to obey the NSW equations on the sloping beach. Based on the hodograph transformation method we have shown that the runup elevation (velocity) is proportional to the half-derivative (three-halves derivative) of the incoming elevation time series at the foot of the slope. This solution is determined either in terms of the inverse Fourier transform or in terms of a simple convolution integral. While the inverse Fourier transform (combined with complex contour integration) is attractive for the case of simple wave forms, the alternative convolution formulation is attractive for more complicated wavetrains.

In the first part of our work, we have considered incident single waves and *N*-waves composed of positive and negative single waves, where the duration and the wave height can be specified separately. As a result of complex contour integration, Cauchy's residue technique and an extension of the convergence of power series via

https://doi.org/10.1017/S0022112009992485 Published online by Cambridge University Press

analytical continuation, we have determined the corresponding temporal variations of the runup elevation, the associated velocity and the breaking criteria in terms of polylogarithmic functions. The resulting analytical solutions are both simple and versatile on a geophysical scale. This part represents an extension of the work by Synolakis (1987) and Tadepalli & Synolakis (1994) in two ways: Firstly, by avoiding the classical solitary wave tie between wavenumber (or frequency) and the wave height to depth ratio, we can actually represent the length- and time-scales which are relevant for geophysical tsunamis. Secondly, we provide solutions for the complete temporal variation of the shoreline motion improving the work of Synolakis (1987) who described the variation only up to the maximum runup for solitary waves, and Tadepalli & Synolakis (1994) who described the variation only up to the maximum rundown of leading depression isosceles waves. Furthermore, we have expressed all the maxima for runup/rundown velocities/elevations as well as the theoretical breaking criteria as a function of the surf-similarity parameter ξ and the incoming wave amplitude over depth ratio A_0/h_0. For non-breaking waves, the isosceles wave will generally lead to runup elevations and velocities higher than any of the other wave forms (when keeping the incident wave crest heights constant).

In the second part of our work, we have considered incoming transient wavetrains generated by monopole and dipole disturbances in the deep ocean. The evolution of these wavetrains, travelling over constant depth in the ocean, is influenced by weak dispersion and is governed by the linear KdV equation. This process has been described by a convolution integral involving the Airy function. When combined with the convolution method for runup, this approach provides a very versatile procedure, which swiftly captures the prevailing features for the entire process starting with an initial disturbance of arbitrary shape in the deep ocean, followed by the long-distance evolution under the influence of weak dispersion, and eventually leading to nonlinear shoaling and runup on a plane sloping beach. We have compared the analytical results with numerical results obtained by a high-order Boussinesq model (using a fixed grid size of 400 m): For the leading long waves in the transient wavetrain (periods of order 10–13 min) we find a good agreement in runup elevation and velocity. Once the main hump of water has passed, the wave components become shorter and shorter while the runup excursion becomes smaller. This situation requires a finer grid size in order to capture the runup with sufficient accuracy, and therefore we notice a growing discrepancy between the analytical solution and the numerical solution. The main features excluded from this approach are those due to (1) effects of two horizontal dimensions, (2) site-specific bottom variation, (3) the possible formation of undular bores due to combined dispersive and nonlinear effects, and (4) wave breaking close to the beach.

First of all, special thanks to Eric Geist for clarifying earlier work on the runup of N-waves and to David Fuhrman for making the numerical simulations applied in figures 9–12. Secondly, we thank the Danish Center for Scientific Computing for providing the invaluable supercomputing time used in the numerical simulations. This work was financially supported by the Danish Technical Research Council (STVF Grant number 9801635). Their support is greatly appreciated.

REFERENCES

Battjes, J. A. 1974 Surf similarity. In *Proceedings of the Fourteenth International Coastal Engineering Conference*, vol. 1, pp. 466–480. ASCE.

https://doi.org/10.1017/S0022112009992485 Published online by Cambridge University Press

Briggs, M. J., Synolakis C. E., Harkins, G. S. & Green, D. R. 1995 Laboratory experiments of tsunami runup on a circular island. *Pure Appl. Geophys.* **144** (3/4), 569–593.

Carrier, G. F. 1971 The dynamics of tsunamis. In *Mathematical Problems in the Geophysical Sciences. Proceedings of the Sixth Summer Seminar on Applied Mathematics, Rennselar Polytechnic Institute, Troy, N.Y. 1970*. American Mathematical Society.

Carrier, G. F. & Greenspan, H. P. 1958 Water waves of finite amplitude on a sloping beach. *J. Fluid Mech.* **17**, 97–110.

Carrier, G. F., Wu, T. T. & Yeh, H. 2003 Tsunami runup and drawdown on a plane beach, *J. Fluid Mech.* **475**, 79–99.

Didenkulova, I. I., Kurkin, A. A. & Pelinovsky, E. N. 2007 Run-up of solitary waves on slopes with different profiles. *Atmos. Ocean. Phys.* **43** (3), 384–390.

Didenkulova, I. I., Zahibo, N., Kurkin, A. A., Levin, B. V., Pelinovsky, E. N. & Soomere, T. 2006 Runup of nonlinearly deformed waves on a coast. *Dokl. Earth Sci.* **411** (8), 1241–1243.

Fuhrman, D. R. & Bingham, H. B. 2004 Numerical solutions of fully nonlinear and highly dispersive Boussinesq equations in two horizontal dimensions. *Intl J. Numer. Methods Fluids* **44**, 231–255.

Fuhrman, D. R. & Madsen, P. A. 2008 Simulation of nonlinear wave runup with a high-order Boussinesq model. *Coast. Engng* **55** (2), 139–154.

Geist, E. L. 1999 Local tsunamis and earthquake source parameters. *Adv. Geophys.* **39**, 117–209.

Geist, E. L. & Yoshioka, S. 1996 Source parameters controlling the generation and propagation of potential local tsunamis along the Cascadia Margin. *Nat. Hazards* **13**, 151–177.

Gjevik, B. & Pedersen, G. 1981 *Run-up of long waves on an inclined plane*. Preprint Series Institute of Mathematics University of Oslo, 25 pp.

Goring, D. G. 1978 Tsunamis – the propagation of long waves onto a shelf. *Tech. Rep.* Kh-R-38. W. M. Keck Laboratory of Hydraulics and Water Resources, California Institute of Technology.

Green, G. 1838 On the motion of waves in a variable canal of small depth and width. *Trans. Camb. Phil. Soc.* **6**, 457–462.

Jensen, A., Pedersen, G. K. & Wood, D. J. 2003 An experimental study of wave run-up at a steep beach. *J. Fluid Mech.* **486**, 161–188.

Kânoğlu, U. 2004 Nonlinear evolution and runup-rundown of long waves over a sloping beach. *J. Fluid Mech.* **513**, 363–372.

Keller, J. B. & Keller, H. B. 1964 Water wave run-up on a beach. *ONR Research Rep.* Contract NONR-3828(00). Department of the Navy, Washington, DC, p. 40.

Kelly, J. J. 2006 *Graduate Mathematical Physics*. Wiley-VCH Verlag, p. 466.

Lamb, H. 1932 *Hydrodynamics*. Cambridge University Press.

Levinson, N. & Redheffer, R. M. 1970 *Complex Variables*. Holden-Day, p. 430.

Lewin, L. 1980 *Polylogarithms and Associated Functions*. North-Holland.

Lewin, L. 1991 *Structural Properties of Polylogarithms*. American Mathematical Society.

Lewy, H. 1946 Water waves on sloping beaches. *Bull. Am. Math. Soc.* **52**, 737–755.

Li, Y. & Raichlen, F. 2001 Solitary wave runup on plane slopes. *J. Waterway Port Coast. Ocean Engng* **127** (1), 33–44.

Li, Y. & Raichlen, F. 2002 Non-breaking and breaking solitary wave run-up. *J. Fluid Mech.* **456**, 295–318.

Li, Y. & Raichlen, F. 2003 Energy balance model for breaking solitary wave run-up. *J. Waterway Port Coast. Ocean Engng* **47**, 47–59.

Liu, P. L.-F., Cho, Y.-S., Briggs, M. J., Kânoğlu, U. & Synolakis C. E. 1995 Runup of solitary waves on a circular island. *J. Fluid Mech.* **302**, 259–285.

Lynett, P., Sitanggang, K. I., Fernández, E. J. R., Wang, X., Zhou, H., Liu, P. L.-F., Mercado, A., Teng, M. & von Hillebrandt-Andrade, C. G. 2008 Experimental investigation into three-dimensional long wave breaking. In *Proceedings of the Thirty-First International Conference on Coastal Engineering,* pp. 1326–1336. Hamburg, ASCE.

Madsen, P. A., Bingham, H. B. & Liu, H. 2002 A new Boussinesq method for fully nonlinear waves from shallow to deep water. *J. Fluid Mech.* **462**, 1–30.

Madsen, P. A. & Fuhrman, D. R. 2008 Runup of tsunamis and long waves in terms of surf-similarity. *Coast. Engng* **55** (3), 209–224.

https://doi.org/10.1017/S0022112009992485 Published online by Cambridge University Press

Madsen, P. A., Fuhrman, D. R. & Schäffer, H. A. 2008 On the solitary wave paradigm for tsunamis. *J. Geophys. Res.* **113**, C12012, 1–22.

Madsen, P. A., Fuhrman, D. R. & Wang, B. 2006 A Boussinesq-type method for fully nonlinear waves interacting with a rapidly varying bathymetry. *Coast. Engng* **53**, 487–504.

Mathews, J. H. & Howell, R. W. 2001 *Complex Analysis for Mathematics and Engineering*. Jones and Bartlett, p. 600.

Mei, C. C., Yue, D. K.-P. & Stiassnie, M. 2005 *Theory and Applications of Ocean Surface Waves*. World Scientific.

Pelinovsky, E. N. & Mazova, R. K. 1992 Exact analytical solutions of nonlinear problems of tsunami wave run-up on slopes with different profiles. *Nat. Hazards* **6**, 227–249.

Synolakis, C. E. 1987 The runup of solitary waves. *J. Fluid Mech.* **185**, 523–545.

Synolakis, C. E. & Bernard, E. N. 2006 Tsunami science before and beyond Boxing Day 2004. *Phil. Trans. R. Soc.* A **364**, 2231–2265.

Synolakis, C. E. & Deb, M. K. 1988 On the maximum runup of cnoidal waves. In *Proceedings of ASCE, 21st Conf. Coastal Engineering*, Costa del Sol, Malaga, Spain, pp. 553–565.

Synolakis, C. E., Deb, M. K. & Skjelbreia, J. E. 1988 The anomaleous behaviour of the runup of cnoidal waves. *Phys. Fluids* **31** (1), 3–5.

Synolakis, C. E., Okal, E. A. & Bernard, E. N. 2005 The megatsunami of December 26, 2004. *Bridge Natl Acad. Engng* **35** (2), 26–35.

Tadepalli, S. & Synolakis, C. E. 1994 The run-up of N-waves on sloping beaches. *Proc. R. Soc. Lond.* A **445**, 99–112.

Tadepalli, S. & Synolakis, C. E. 1996 Model for the leading waves of tsunamis, *Phys. Rev. Lett.* **77**, 2141–2145.

Tonkin, S., Yeh, H., Kato, F. & Sato, S. 2003 Tsunami scour around a cylinder. *J. Fluid Mech* **496**, 165–192.

Weisstein, E. W. 2005 Analytic continuation and polylogarithm. *Mathworld* - A Wolfram Web Resource.

Whitham, G. B. 1974 *Linear and Nonlinear Waves*. Pure and Applied Mathematics, Wiley-Interscience.

Wood, D. C. 1992 The computation of Polylogarithms. *Tech. Rep.* **15–92**. University of Kent Computing Laboratory, University of Kent, Canterbury, UK, p. 20.

Yeh, H., Liu, P. L.-F., Briggs, M. & Synolakis, C. E. 1994 Propagation and amplification of tsunamis at coastal boundaries. *Nature* **372**, 353–355.

https://doi.org/10.1017/S0022112009992485 Published online by Cambridge University Press